Natural Resources Canada | Ressources naturelles Canada

GEOLOGICAL SURVEY OF CANADA
OPEN FILE 8334

Temporal and geochemical evolution of the Guichon Creek Batholith and Highland Valley porphyry copper district, British Columbia: Implications for generation and tectonic setting of porphyry systems

J.B. Whalen, W.J. Davis, and R.A. Anderson

2017

GEOLOGICAL SURVEY OF CANADA
OPEN FILE 8334

Temporal and geochemical evolution of the Guichon Creek Batholith and Highland Valley porphyry copper district, British Columbia: Implications for generation and tectonic setting of porphyry systems

J.B. Whalen, W.J. Davis, and R.A. Anderson

2017

Permanent link: https://doi.org/10.4095/306147

This publication is available for free download through GEOSCAN (http://geoscan.nrcan.gc.ca/).

Recommended citation

Whalen, J.B., Davis, W.J. and Anderson, R.A., 2017. Temporal and geochemical evolution of the Guichon Creek Batholith and Highland Valley porphyry copper district, British Columbia: Implications for generation and tectonic setting of porphyry systems; Geological Survey of Canada, Open File 8334, 1 .zip file. https://doi.org/10.4095/306147

Publications in this series have not been edited; they are released as submitted by the author.

Temporal and Geochemical Evolution of the Guichon Creek Batholith and Highland Valley Porphyry Copper District, British Columbia: Implications for Generation and Tectonic Setting of Porphyry Systems.

J.B. Whalen[1,3], W.J. Davis[1] and R.A. Anderson[2]

[1] *Geological Survey of Canada, 601 Booth Street, Ottawa, ON, Canada, K1A 0E8*

[2] *Geological Survey of Canada, 625 Robson Street, Vancouver, British Columbia, Canada, V6B 5J3*

[3] *Corresponding author: email, Joe.Whalen@Canada.ca*

Abstract

Guichon Creek Batholith, a Late Triassic, calc-alkaline composite batholith of the Nicola arc, British Columbia, hosts major porphyry copper deposits of the Highland Valley district. U-Pb zircon and Ar-Ar age dating of the main intrusive phases of this normally compositionally zoned batholith indicate that it evolved over a 7 M.y. period (215.6 ± 0.5 to 208.6 ± 0.6 Ma). The batholith consists of two distinct geochemical suites, the barren pre-211 Ma Highland Valley, and the mineralized post-211 Ma Bethlehem suite. Ages of host intrusion and a cross-cutting, post-mineralization dyke date the Bethlehem deposit to within a <1 M.y. period at ~210 Ma. This event predates the Bethsaida pluton, host to Valley, Lornex and Highmount deposits. These younger deposits formed after 209.1 ± 0.3 Ma, prior to or synchronously with the Gnawed Mountain porphyry at 208.6 ± 0.6 Ma. Ar-Ar and U-Pb ages are generally similar, indicating short-lived and rapidly cooled magmatic/hydrothermal systems. Published Re-Os molybdenite ages at Valley suggest a third mineralizing event at 206.5 Ma.

Mineralization is linked to the change in magma composition between the Highland Valley and Bethlehem suites, both of which have distinctive high Sr/Y, La/Yb and Gd/Yb signatures. The Bethlehem suite is more calcic, hydrous and oxidized than Highland Valley suite. Both suites were likely derived by melting hydrous, metal-enriched mafic lower crustal cumulates residual from earlier arc magmatism. Partial melting of such protoliths is thought to have been triggered by arc-arc collision, followed by slab detachment and upwelling of hot athenospheric mantle-derived mafic magmas. Termination of Triassic arc calc-alkaline volcanism overlapped with the ca 216 Ma outer mafic Border phase. Emplacement (211-208 Ma) of batholith interior phases was accompanied by porphyry Cu formation at 210 and ~208 Ma. Based on this study, the fertile Guichon Creek Batholith represents a template for understanding porphyry deposit formation and distribution that can facilitate exploration targeting.

Introduction

The timing of major Cu-porphyry systems in Miocene, circum-Pacific arc settings is often thought to be linked to major tectonic changes in the associated subduction system as are changes in the geochemical characteristics of cogenetic plutonic suites (Kay et al., 1999; Cooke et al., 2005; Hollings et al., 2005; Hildebrand and Whalen, 2014, 2017). Tectonic events, including ridge subduction, accretion, changes in slab dip or slab failure have been suggested to trigger changes in sub-arc melting processes and compositions of derived magmas that favour magmatic transport of metals and the development of hydrothermal systems within the upper part of the arc system. Therefore, specific time periods within an arc's tectonic evolution may have greater probabilities of hosting economic porphyry systems and their cogenetic magmas may exhibit distinctive geochemical characteristics. Identifying these tectonically favourable time periods in ancient arc systems and geochemical discrimination of fertile plutonic suites are critical elements in evaluating regional scale prospectivity for major porphyry mineralization.

The Highland Valley District (HVD), the largest porphyry camp in Canada,, has produced as of 2013, ~ 6.5 Mt of Cu (Byrne et al., 2013) with proven and probable ore reserves of 546.6 Mt @0.29% Cu and 0.008% Mo (http://www.teck.com/media/2017-AIF.pdf). The deposits are hosted by the Guichon Creek Batholith (GCB), a late Triassic calc-alkaline intrusive complex within the Nicola arc, Quesnel Terrane, of the Intermontane belt, southeastern British Columbia (Fig. 1). The Nicola arc is also well known for hosting several Cu-Au porphyry systems, such as Ajax and Afton and Mount Polley, that are associated with latest Triassic to earliest Jurassic alkaline intrusions of the Copper Mountain plutonic suite (CMPS; Lang et al., 1995; Woodsworth et al., 1991). Despite the importance of the Guichon Creek Batholith as host to major copper deposits, modern geochemical analyses are lacking and little is known about the precise timing and duration of magmatism and mineralization, information critical to understanding its petrogenesis and relationship to the tectonic evolution of southern Quesnel Terrane. We present new high-precision U-Pb and Ar-Ar geochronological data, Nd isotopic data and high-quality geochemical analyses in order to evaluate: (a) the temporal and petrochemical development of this batholith and its relationship to mineralizing systems; and (b) constrain its larger scale tectonic context and relevance for porphyry deposit formation and distribution in general.

It should be noted that after our study was completed, there was a delay of over six years during which period, without our knowledge, an MSc. study was carried out that essentially duplicated almost all our research (D'Angelo, 2016). As the results of that thesis research are at an advanced stage in publication with Economic Geology journal (D'Angelo et al., in press), we decided that it was appropriate that our unpublished manuscript should be released as a Geological Survey of Canada Open File.

Regional Geological Context

The Guichon Creek Batholith occurs within the Intermontane Belt of southeast British Columbia, which is characterized by Late Paleozoic to mid-Mesozoic subduction-related volcanic and plutonic rocks

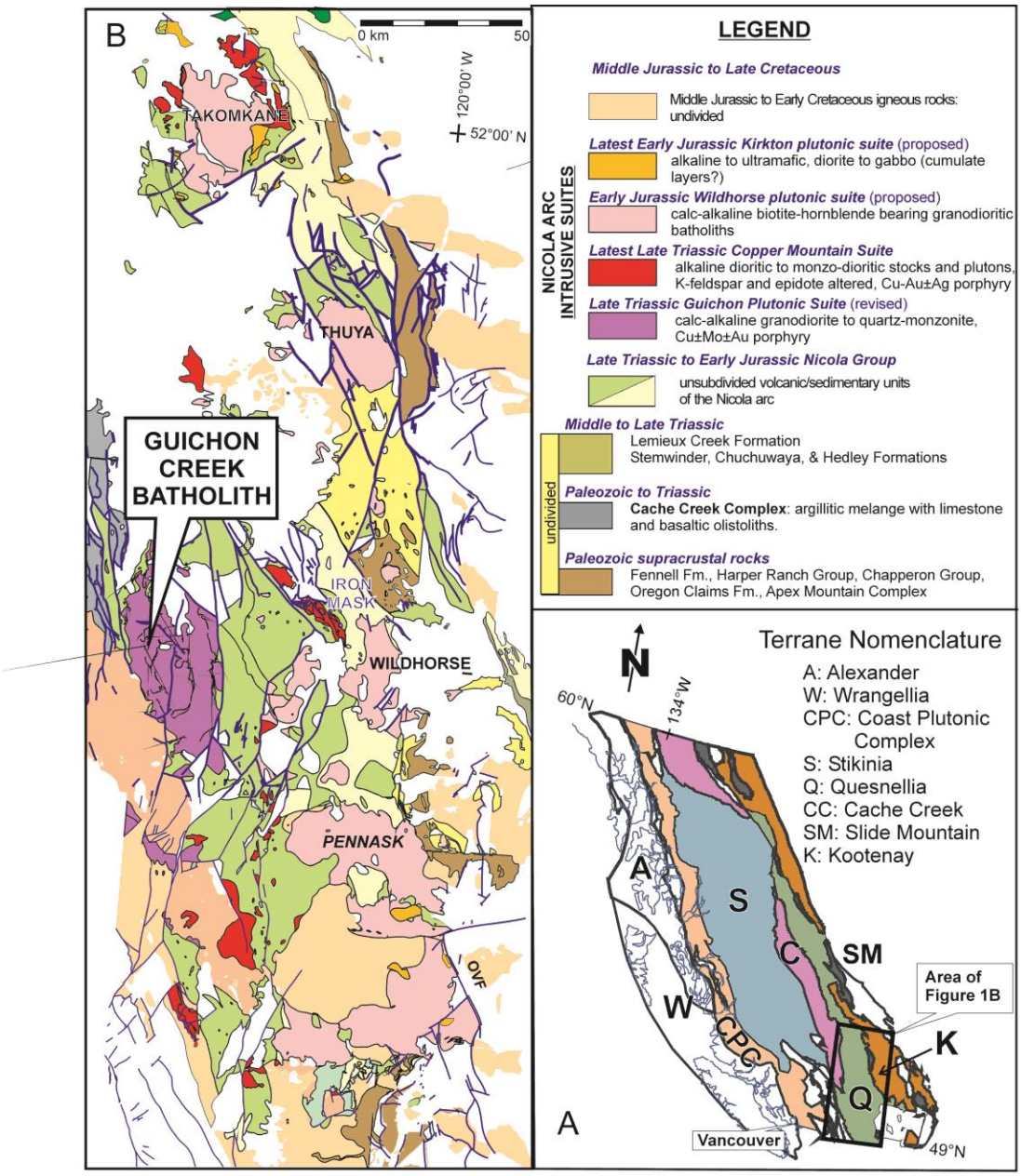

Figure 1. (a) Terrane map of the Cordilleran orogen, British Columbia, Canada; and (b) Regional geological setting of Guichon Creek Batholith within Nicola arc of the Quesnel terrane. (modified from Breitspecher et al., 2007)

(Stikinia and Quesnel terranes) and a related, medial accretionary complex, the oceanic Cache Creek terrane (Fig. 1). The Quesnel terrane Mesozoic Nicola Group volcanic sequence, is fault-bounded with accretionary rocks of the Cache Creek Terrane to the west and Mesozoic to Paleozoic rocks of the pericratonic Kootenay Terrane to the east. Mafic volcanic and sedimentary rocks of the intervening Slide Mountain Terrane are interpreted to have formed in a Late Paleozoic marginal basin that separated Quesnel from North America (Monger and Price, 2002; Colpron and Nelson, 2007). The paleogeographic association of Intermontane Belt terranes remains controversial as development of their arc rocks has been

interpreted to either pre-date, or to be coeval with their accretion as terranes by eastward-dipping subduction to the western edge of North America at *ca.* 185 to 180 Ma (Monger et al., 1982; Ricketts et al., 1992; Struik et al., 2001; Monger and Price, 2002, Colpron et al., 2007, Logan and Mihalynuk, 2014). In contrast, Johnston (2008) has suggested that these terranes formed within an intra-oceanic arc environment 1000s of km off-board. In Late Triassic, they were involved in a major intra-oceanic collisional/orogenic event during which the North America autochthon remained a distal unaffected west-facing passive margin far to the east. At this time, Quesnel Terrane overthrust the pericratonic assemblages along major east-verging thrust faults. Terrane amalgamation to form an enormous ribbon continent (Rubia Superterrane of Hildebrand (2013)) was followed by: (a) termination of arc magmatism; (b) slab-failure; (c) emplacement of Early Jurassic post-tectonic plutons into Quesnel; (d) major Early to Middle Jurassic uplift and erosion of the deeply buried pericratonic margin; and (e) Early Jurassic molasse deposition across Stikinia-Quesnel (op. cit.). However, Hildebrand (2013) interprets this major terrane accretion event to be Jurassic, with the pericratonic Kootenay terrane being pulled beneath Quesel between 187 and 185 Ma, significantly latter than in the model of Johnston (2008). The Rubia Superterrane subsequently collided with North America by westward-dipping subduction, initially at ~124 Ma (Sevier orogeny), but ultimately at ~80-75 Ma (Laramide orogeny) (Hildebrand, 2010, 2013).

In southern Quesnel Terrane, the Guichon Creek Batholith (GCB) is associated with the Late Triassic to Early Jurassic, mainly volcanic, Nicola Group that developed from approximately ~220 Ma to 190 Ma. The group's magmatic record can be subdivided into three main phases of activity. The first phase into which the GCB was emplaced is represented by low-K calc-alkaline volcanic rocks of the western Nicola Group (Mortimer, 1987). Regionally, the rocks are not well dated but are interpreted to be late Carnian (~217-224 Ma) to early to middle Norian (210-217 Ma) arc-type volcanic rocks, based on paleontological evidence (Beatty et al., 2006, Ray and Dawson, 1994). In the Merritt area, a few kilometres southeast of the GCB, a submarine sequence in the Nicola Group yields Upper Triassic (lower and middle Norian) bivalves and conodont fauna and a preliminary U-Pb date of about 224 Ma (Diakow, 2010; M.J. Orchard, personal communication, August 2010). The older (ca. 216 Ma) outer GCB mafic Border phase maybe consaguineous with, or only slightly younger than, its Nicola Group mafic volcanic wall rocks. The youngest plutonic rocks related to this western magmatism are represented by granodioritic to tonalitic 211-208 Ma, GCB phases, which evolved from calc-alkalic to calcic over a ca. 3 Ma time period (see Figs. 3, 4b and 13). This magmatism ceased at ~208 Ma and is separated from the middle and upper sections of the Nicola Group by an unconformity at the type-section (Schau, 1970). Mortimer (1987) also documented a minor component of volcanic rocks characterized by non-arc within plate signatures within middle sections of the Nicola Group. Upper Nicola Group magmatism developed at approximately 204 Ma (Mortimer, 1987; Parrish and Monger, 1992; Breitsprecher et al., 2007) to the east of the GCB. It consists mainly of subaerial intermediate to felsic high-K to shoshonitic volcanism and cogenetic plutonism of the Copper Mountain suite (see Figs. 3 and 4) that host important Cu-Au porphyry systems (e.g. Ajax / Afton in the

Iron Mask Batholith; Mount Polley, Copper Mountain, Logan et al., 2007; Logan and Mihalynuk, 2014).

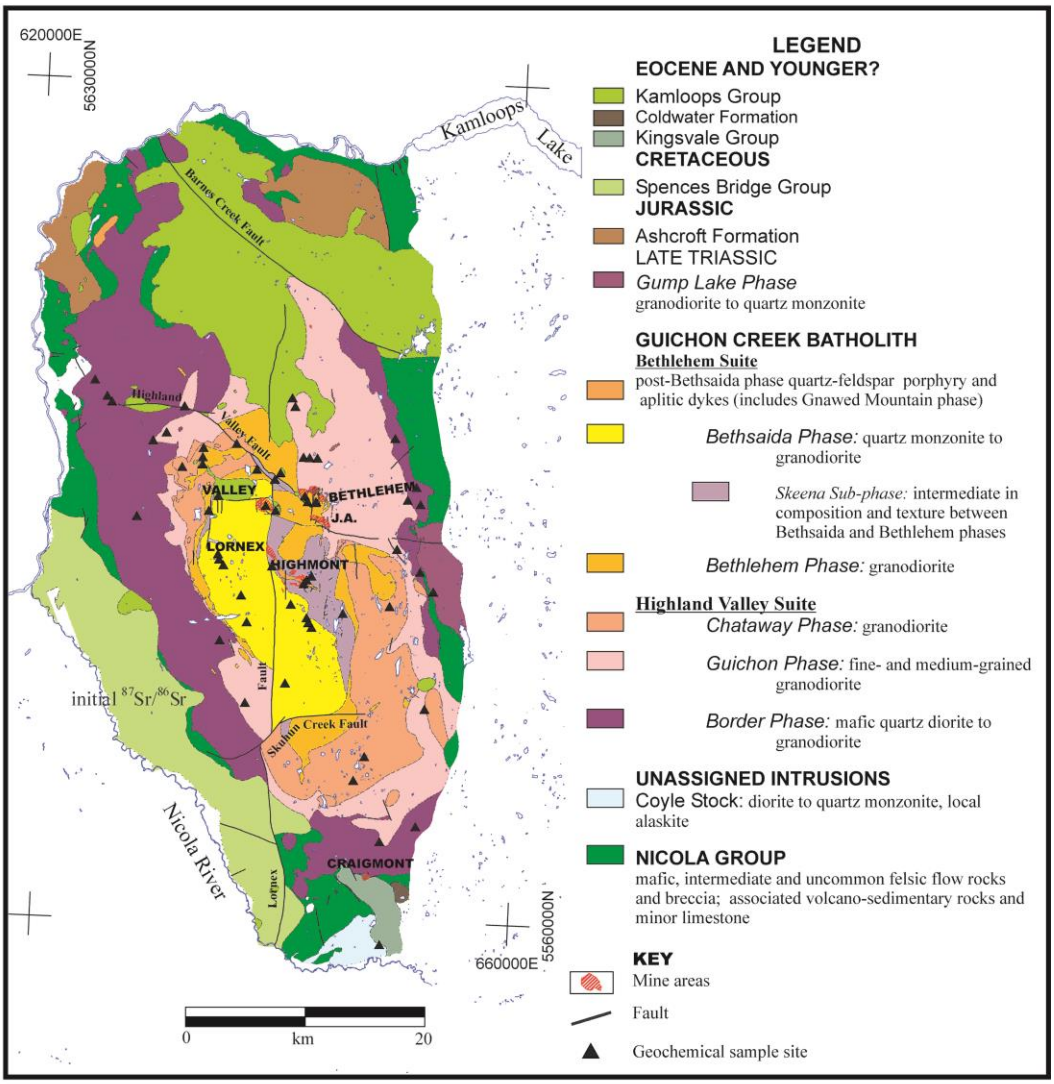

Figure 2. Geology of the Guichon Creek Batholith showing mineral deposit and geochemical plus geochronological sample locations. Figure modified from Figure 7 of Anderson et al. (2012).

Guichon Creek Batholith

Geological context

The Guichon Creek Batholith (GCB) is a large (surface area of about 1000 km^2), composite body which is variably covered by glacial deposits, with its northern part unconformably overlain by Eocene volcanic rocks of the Kamloops Group. Although its margin is mostly covered by these younger deposits, the semi-concordant, domal batholith is considered to have intruded Mississippian to Upper Triassic Cache Creek Complex and lower Nicola Group sedimentary rocks and possible cogenetic island arc volcanic rocks (e.g., Monger and McMillan (1984) and references therein). Based on textural and compositional

criteria, McMillan (1985) originally subdivided the batholith into four phases, which in relative decreasing age, included the Border, Highland Valley, Bethlehem and Bethsaida phases. As well, he recognized the Guichon and Chataway 'varieties' within the Highland Valley phase, and the Skeena 'variety' within the Bethsaida phase. Contacts between the phases, though locally sharp, are commonly gradational and define an annular zoning with the older phases towards the outer margins of the batholith and the younger phases within the central area. Compositional variation within the GCB exhibits a rough normal zoning from outer older diorite/gabbro to inner younger granodiorite/tonalite phases.

Mid- to upper crustal emplacement is suggested by: interphase intrusive relations and dykes; probable semi-concordant to discordant granitoid-country rock contacts; intrusion into slightly older Nicola Group volcano-sedimentary country rocks; a 0.2-0.8 km wide albite-epidote to hornblende hornfels facies metamorphic aureole; and batholithic fragments in the Lower to Middle Jurassic Ashcroft Formation (Northcote, 1969; McMillan, 1976). The latter provides evidence for quite rapid uplift and erosion of the GCB as does unconformably cover of its northern portion by Eocene age volcanic rocks of the Kamloops Group (Fig. 2).

The batholith's northerly elongation suggests control by basement structures manifest in syn- and post-intrusion faults (Hollister et al., 1975, McMillan, 1976; McMillan and Johan, 1981). Important faults in the batholith trend north (e.g., Lornex and Guichon Creek faults) or northwest (e.g., Barnes Creek, Highland Valley and Skuhun Creek faults). The Valley and Lornex deposits are similar and may have been structurally controlled and (or) later offset by dextral movement along Lornex and Highland Valley faults (Hollister et al., 1975; McMillan, 1976). Interpretation of geological and geophysical observations, including gravity, magnetic, velocity and Lithoprobe seismic reflection data, indicate the GCB to be a funnel-shaped feature extending to depths of ~10 km (Roy and Clowes, 2000). Except for the Valley-Lornex deposits which are off-set to the west of the gravity low stem by ~5 km, GCB mineral deposits are located in the center of the structure above the stem of the batholith and near the intersection of the major brittle structures described above.

The different plutonic units define two geochemical suites (McMillan, 1985; see below). Herein we refer to these as (1) the Highland Valley suite (HVS), which includes the earlier Border and younger Guichon and Chataway phases, and (2) the Bethlehem suite (BS), which includes the Bethlehem and Bethsaida phases and the Skeena subphase plus various felsic porphyry dyke types, the largest of which is the Gnawed Mountain subphase (Fig. 2). Earlier geochemical studies (McMillan and Johan, 1981; McMillan, 1985; and references therein) documented discontinuities in elemental distribution trends between older HVS and younger BS plutonic phases.

Our geochemical data for the Guichon Creek Batholith (GCB) are shown in Figure 3 on the IUGS-based normative Q'-ANOR granitoid rock classification diagram of Streckeisen and LeMaitre (1979). In

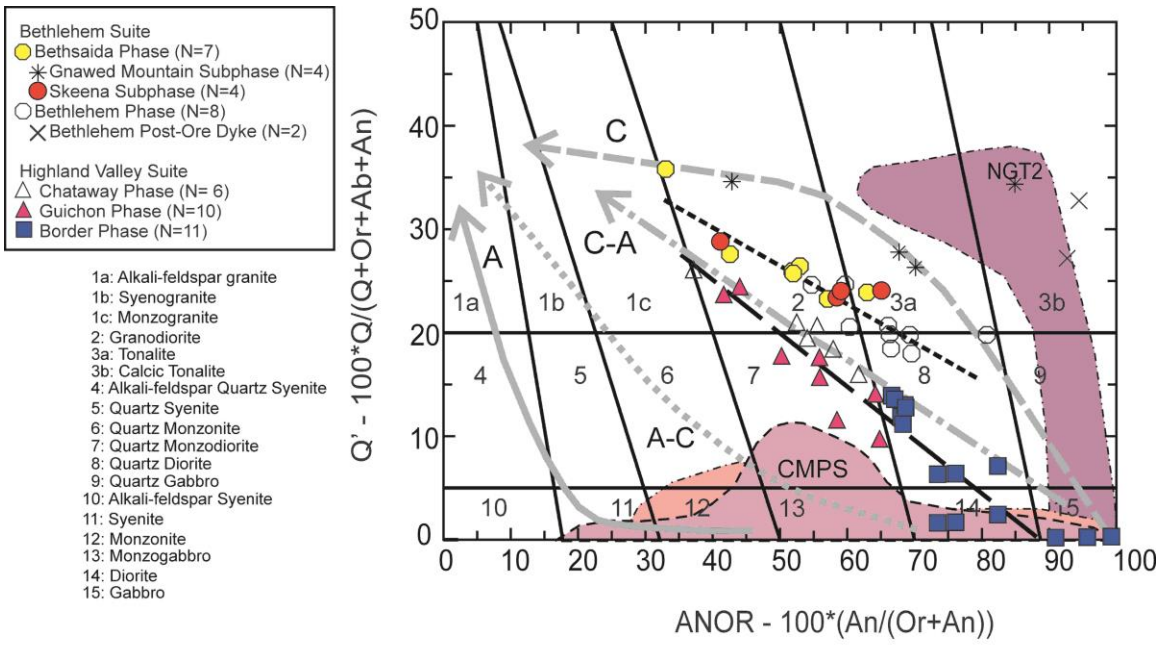

Figure 3. Guichon Creek Batholith plutonic rock samples plotted on the IUGS-based CIPW normative Q - ANOR classification diagram (Streckeisen and LeMaitre, 1979), with samples subdivided as shown in Fig. 2 and the symbol legend. Inferred trends are shown for the Chataway and Guichon phases of the Highland Valley suite (HVS) and the major non-dyke phases of the Bethlehem suite (BS). Note that the HVS trend has been projected to lower silica levels through mafic Border phase compositions. Also shown is the field for the ca 204 200 Ma Au-hosting alkaline Copper Mountain plutonic suite (CMPS) (61 analyses from Schroeter, 1995) and compositional trends for different plutonic suites (A = alkalic; A-C = alkali-calcic; C-A = calc-alkalic; and C = calcic) from Whalen and Frost (2013).

general, the HVS is more mafic. The Border phase consists of diorite/gabbro to quartz diorite with hornblende, biotite, locally two pyroxenes, and magnetite as mafic minerals. Exposures vary from texturally and compositionally homogeneous to containing abundant finer-grained, ovoid, comagmatic mafic inclusions, providing evidence for magma mixing. Locally, Nicola mafic volcanic inclusions are common within the Border phase. The Guichon and Chataway phases exhibit similar quartz monzodiorite to granodiorite compositions and contain hornblende, frequently cored by clinopyroxene, biotite and magnetite. The Chataway phase exhibits a distinctive spotted texture produced by stubby euhedral hornblende. The BS is generally more felsic in composition relative to the HVS. The Bethlehem phase ranges from quartz diorite to granodiorite in composition and contains distinctive plagioclase-poikiolitic hornblende and lesser biotite and magnetite. The younger Bethsaida phase ranges from tonalite to granodiorite and contains biotite, hornblende and magnetite. It is characterized by 5-8 mm ovoid quartz and large, euhedral biotite books. The compositionally similar Skeena subphase is texturally and spatially transitional between the Bethlehem and Bethsaida phases. The Gnawed Mountain subphase, as sampled at a number of locations, including within and adjacent to the Highmont open pit, is a homogeneous biotite-

quartz-feldspar porphyry, that ranges from tonalitic to granodioritic in composition. Generally, phases

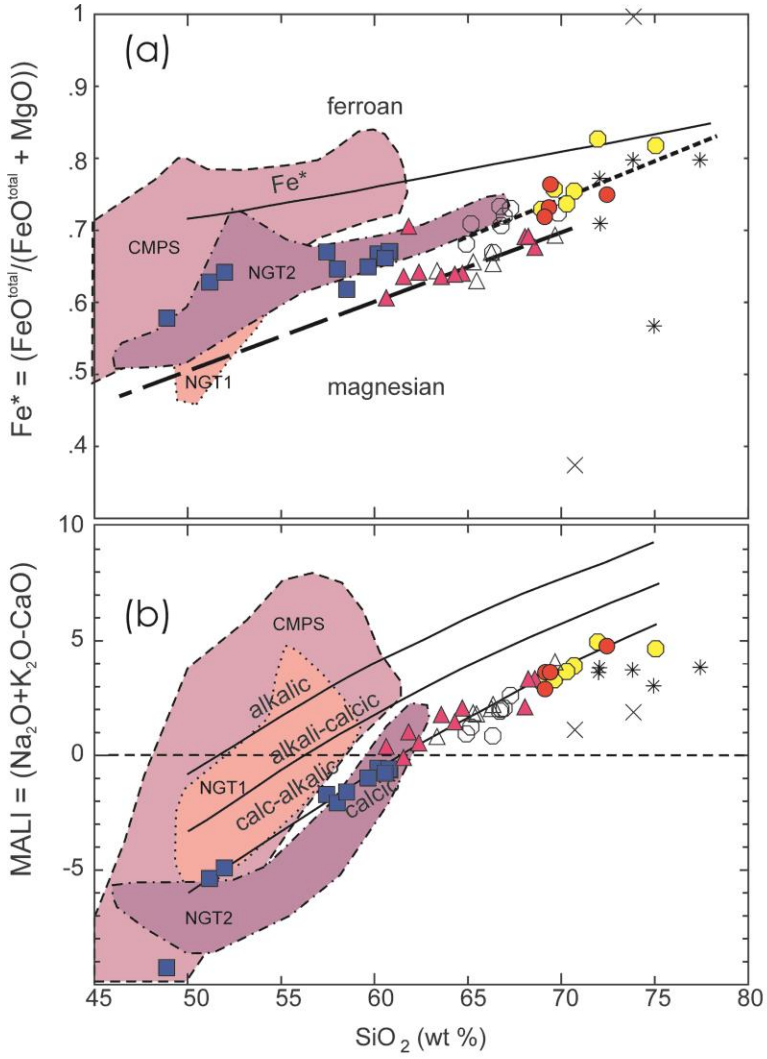

Figure 4. Guichon Creek Batholith rock samples plotted on the: (a) $FeO^{total}/(FeO^{total} + MgO)$ (or Fe*) vs. SiO_2 and (b) Na_2O+K_2O-CaO (or MALI) vs. SiO_2 granitic rock classification diagrams of Frost et al. (2001). In (a) the boundary between ferroan and magnesian plutons has been modified, as suggested by Frost and Frost (2008). Inferred trends and compositional fields, as in Fig. 3. Also shown are fields for Nicola Group type 1 204-200 Ma high-K to shoshonitic lavas (NGT1; N=9) and type 2 224-210 Ma low-K calc-alkaline lavas (NGT2; N=8) from Mortimer (1987).

within the HVS have higher magnetic susceptibilities (e.g., 20-60 10^{-3} SI) compared with Bethlehem Suite rocks (1-20 10^{-3} SI). Excellent photographs that document distinctive textural features of these various GCB plutonic units are presented in Figures 6 and 7 of Casselman et al. (1995).

Mineralization

The Highland Valley District, the largest group of operating Cu mines in Canada, produces Cu with Mo, Ag, and Au from major vein- and fracture-controlled ore deposits (Valley, Lornex, Highmont,

Bethlehem and JA). The deposits occur within the central part of the batholith where they are hosted by the Bethlehem, Skeena, Bethsaida and Gnawed Mountain phases, but smaller deposits (Krain and South Seas) occur within the older Guichon phase (Fig. 2). According to McMillan (1985), there were two porphyry deposit-forming events within the GCB, an earlier pre-Bethsaida event that produced the Bethlehem ore bodies, plus smaller Krain and South Seas deposits, and a second more significant post-Bethsaida event, during which the Valley, Lornex, and Highmont deposits formed. Within the Bethlehem deposits McMillan (1985) mapped various felsic dyke suites, one of which he interpreted as post-dating mineralization, but pre-dating the Bethsaida phase (McMillan et al., 2009).

Mineralization at Highland Valley has a Cu-Mo association with little gold and is hosted in calc-alkalic to calcic plutonic rocks (Figs. 3 and 4b). This contrasts with younger ca 204-200 Ma Cu-Au porphyry mineralization associated with the alkaline Copper Mountain plutonic suite (CMPS), such as the Iron Mask Batholith and at Mount Polley (McMillan et al., 1996; Lang et al., 1995; Mortimer et al., 1986; Ray et al., 1986; field highlighted in Figs. 3 and 4).

Previous Geochronology

Few, high-precision geochronological data are available to calibrate the magmatic-hydrothermal evolution of the Guichon Creek Batholith (GCB). The published estimate of the crystallization age was provided by a Late Triassic U-Pb zircon age of 210 ± 3 Ma (Mortimer et al. 1990) for the Guichon phase of the Highland Valley suite. Numerous K-Ar analyses carried out in the 1960s and 1970s (White et al., 1967; Branchflower, 1971; Wanless et al., 1965, 1968; Wanless, 1973; Jones et al., 1973) yielded a small range of imprecise ages at around 200 Ma. A total of 29 K-Ar analyses on biotite within various plutonic phases (McMillan et al., 2009) range from 212 Ma to 190 Ma (recalculated with accepted decay constants) with a weighted mean K-Ar age of ~202 Ma. However, there is no systematic correspondence between intrusive phase and age. Eight hornblende analyses exhibit a similar range with seven of eight hornblende K-Ar analyses at ca. 201 Ma. K-Ar ages of hydrothermal sericite associated with mineralization yield a range of imprecise ages between 205 and 190 Ma. Collectively these data demonstrate that mineralization is broadly correlative with late Triassic magmatic activity but are insufficient to assess the relationship between magmatism and hydrothermal activity within the GCB.

More recently Ash et al. (2007) reported precise Ar-Ar step-heating ages for magmatic biotite and hydrothermal sericite from the Valley pit of 207 ± 2 Ma and 204 ± 2 Ma, respectively (see McMillan et al. (2009) for sample locations). In addition, they report duplicate Re-Os ages for molybdenite from the Valley pit of 206.7 ± 1.5 and 205.8 ± 1.5 Ma and interpret mineralization to have occurred between ca. 207 and ca. 204 Ma. The new data presented here provide the regional temporal and petrological frameworks to link the magmatic and hydrothermal history of the GCB.

U-Pb Geochronology

Analytical techniques

Thermal Ionisation U-Pb Analyses

Heavy mineral concentrates were prepared by standard techniques (crushing, grinding, Wilfley™ table, heavy liquids), and sorted by magnetic susceptibility using a Frantz™ isodynamic separator. All zircon fractions were air abraded (Krogh, 1982) except those from the Border phase which were chemically abraded following methods of Mattinson (2005). Isotopic and U-Pb compositional data were determined by isotope dilution thermal ionization mass spectrometry at the Geochronology Laboratory, Geological Survey of Canada. Sample dissolution and chemical methods are described in Parrish et al. (1987). Individual crystals were selected under binocular microscope to avoid inclusions and other imperfections, spiked with a mixed ^{205}Pb-^{233}U-^{235}U tracer solution calibrated to ±0.1% against a gravimetric solution, and dissolved in high-pressure bombs in HF-HNO3. Data reduction and error propagation follow methods outlined in Roddick (1987). U and Pb isotopic ratios were measured using a Finigan Mat Trition mass spectrometer operated in static multi-collection mode. The ^{205}Pb, ^{206}Pb, ^{207}Pb, and ^{208}Pb isotopes were measured simultaneously in Faraday collectors, with ^{204}Pb in an axial secondary electron multiplier. Faraday-multiplier gain was monitored and corrected by peak jumping ^{205}Pb into the axial cup. A Pb mass fractionation correction of 0.1± 0.04%/amu was applied as determined by replicate analyses of the NBS981 standard (see Table 1). U fractionation was corrected using the ^{233}U-^{235}U double spike and was typically in the range of 0.12%/amu.

SHRIMP U-Pb Methods

SHRIMP analytical procedures followed those described by Stern (1997), with standards and U-Pb calibration methods following Stern and Amelin (2003). Briefly, zircons were cast in 2.5 cm diameter epoxy mounts along with fragments of the GSC laboratory standard zircon (z6266, with ^{206}Pb/^{238}U age = 559 Ma). The mid-sections of the zircons were exposed using 9, 6, and 1 µm diamond compound, and the internal features of the zircons (such as zoning, structures, alteration, etc.) were characterized in back-scattered electron mode (BSE) utilizing a Zeiss Evo 50 scanning electron microscope. Mount surfaces were evaporatively coated with 10 nm of high purity Au. Analyses were conducted using an $^{16}O^-$ primary beam, projected onto the zircons at 10 kV. The sputtered area used for analysis was ca. 25 µm in diameter with a beam current of ca. 8 nA. The count rates at ten masses including background were sequentially measured over 5 scans with a single electron multiplier and a pulse counting system with deadtime of 23 ns. Off-line data processing was accomplished using customized in-house software. The 1σ external errors of ^{206}Pb/^{238}U ratios reported in the data table incorporate a ± 1.0 % error in calibrating the standard zircon (see Stern and Amelin, 2003). No fractionation correction was applied to the Pb-isotope data; common Pb correction utilized the Pb composition of the surface blank (Stern, 1997). Isoplot v. 3.00 (Ludwig, 2003) was used to generate concordia plots and calculate weighted means. The error ellipses on the concordia diagrams, and the weighted mean errors are reported at 2σ.

Analyses of a secondary zircon standard (Temora 2) were interspersed between the sample analyses to verify the accuracy of the U-Pb calibration. Using the calibration defined by the z6266

standard, the weighted mean $^{206}Pb/^{238}U$ age of fourteen SHRIMP analyses of Temora 2 zircon is 415.6 ± 4.6 Ma (95% conf.). The accepted $^{206}Pb/^{238}U$ age of Temora 2 is 416.5 ± 0.22 Ma (Black et al. 2004).

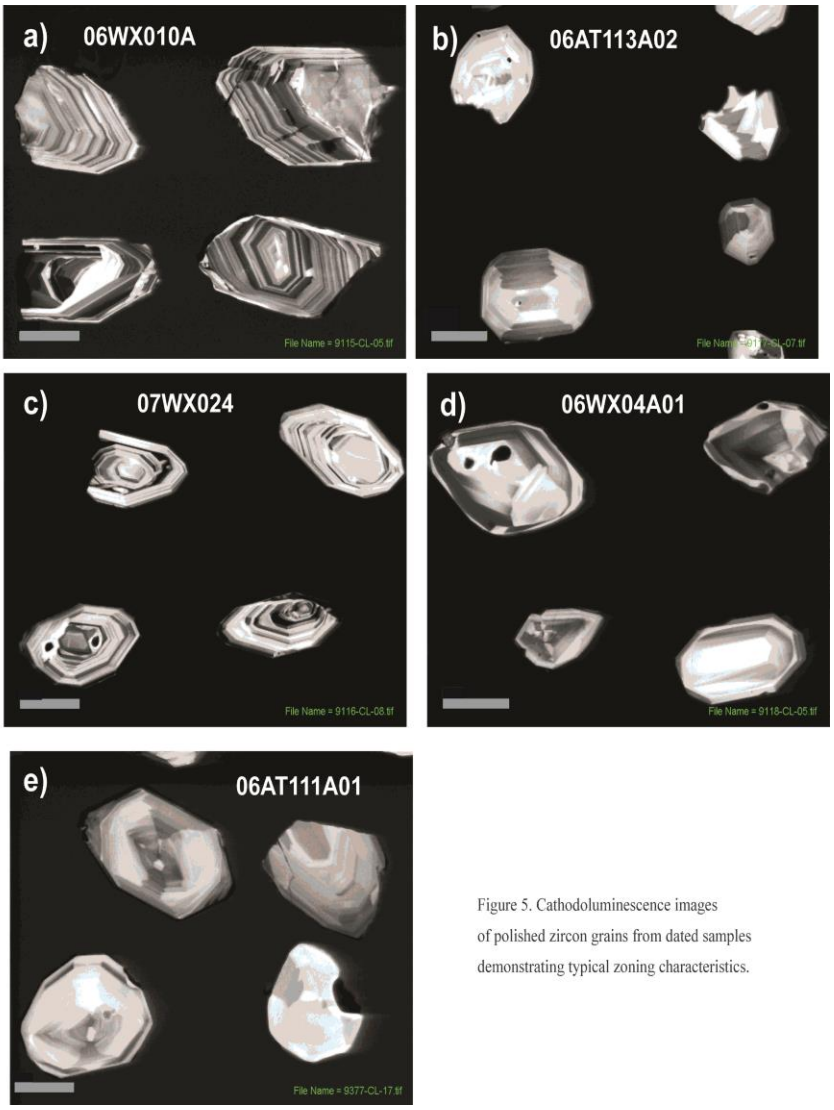

Figure 5. Cathodoluminescence images of polished zircon grains from dated samples demonstrating typical zoning characteristics.

U-Pb geochronological results

Highland Valley Suite

Border phase (sample 06WX-014-A01): This Border phase diorite sample was collected from a roadcut through the northwest lobe of the Border phase (Fig. 2). Zircon occurs as clear colorless euhedral prisms. Six single grain analyses yield $^{206}Pb/^{238}U$ ages ranging from 215.0 ± 0.5 to 217 ± 0.6 Ma. The six analyses

Table 1. U-Pb analytical data, thermal ionisation mass spectrometry

Fraction	Description[1]	# gr	Size	Wt.	U[2]	Pb,	Pbc	Atomic Ratios[4] (± 1sigma error)						Age (Ma, ± 2sigma error)					
								$^{208}Pb/$ ^{204}Pb	$^{206}Pb/$ ^{204}Pb	$^{207}Pb/$ ^{235}U	±	$^{206}Pb/$ ^{238}U	±	Correlation Coefficient[5]	$^{206}Pb/$ ^{238}U	±	$^{207}Pb/$ ^{235}U	±	% Discord.
				(µg)	(ppm)	(ppm)	(pg)												
06WX-014-A01 Border Phase Diorite, Guichon Batholith (z11227) 10 625674E 5604351N UTM NAD83																			
A20-1 (Z)	Z,Co,Clr,Eu,Pr,CA,M0°	1	250	59.4	93	3	2.8	4207.9	0.12	0.23715	0.00032	0.03405	0.00004	0.8551125	215.8	0.5	216.1	0.5	1.43
A20-2 (Z)	Z,Co,Clr,Eu,Pr,CA,M0°	1	200	22	77	3	1.31	2762.3	0.13	0.23693	0.00035	0.03401	0.00003	0.7929969	215.6	0.4	215.9	0.6	1.62
A20-3 (Z)	Z,Co,Clr,Eu,Pr,CA,M0°	1	200	22.2	96	3	1.4	3262.8	0.12	0.23927	0.00038	0.03425	0.00004	0.7759589	217.1	0.6	217.8	0.6	4
A20-4 (Z)	Z,Co,Clr,Eu,Pr,CA,M0°	1	200	27.8	74	3	1.52	2905.8	0.11	0.23791	0.00035	0.03412	0.00004	0.8012209	216.3	0.5	216.7	0.6	2.49
A20-5 (Z)	Z,Co,Clr,Eu,Pr,CA,M0°	1	200	33.1	78	3	6.37	192.3	0.12	0.24069	0.0047	0.0339	0.00012	0.5986335	214.9	1.5	219	7.7	18.71
A20-6 (Z)	Z,Co,Clr,Eu,Pr,CA,M0°	1	225	51.4	150	5	1.61	10149.1	0.12	0.23608	0.00035	0.03391	0.00004	0.9356212	215	0.5	215.2	0.6	1.2
06AT111A01 Gnawed Mountain Porphyry (Z9115) 10 639631E 5589695N UTM NAD83																			
ZA1 (Z)	Z,Co,Clr,Eu,Pr,Abr,M0°	5	164	10	146	5	17	190.5	0.10	0.2298	0.0028	0.03285	0.00009	0.6402	208.4	1.1	210.0	4.6	8.9
ZA2 (Z)	Z,Co,Clr,Eu,Pr,Abr,M0°	7	137	12	111	4	8	375.5	0.10	0.2291	0.0011	0.03287	0.00005	0.6765	208.5	0.6	209.5	1.8	5.6
ZA3 (Z)	Z,Co,Clr,Eu,Pr,Abr,M0°	12	112	10	135	4	10	290.5	0.11	0.2311	0.0015	0.03294	0.00007	0.6863	208.9	0.8	211.1	2.4	11.6
ZB1 (Z)	Z,Co,Clr,Eu,Pr,Abr,M0°	4	190	13	105	3	3	976.4	0.11	0.2284	0.0006	0.03292	0.00004	0.6783	208.8	0.5	208.9	1.0	0.4
06WX04A01 Bethsaida Phase, Guichon Batholith (Z9116) 10 637025E 5587333N UTM NAD83																			
ZA1 (Z)	Z,Co,Clr,Eq,Eu,Abr,Dia	8	160	10	207	7	3	1655.4	0.12	0.2275	0.0019	0.03284	0.00026	0.9790	208.3	3.3	208.1	3.1	-1.2
ZA3 (Z)	Z,Co,Clr,Eq,Eu,Abr,Dia	31	116	50	197	7	7	3029.7	0.11	0.2289	0.0003	0.03296	0.00003	0.8686	209.0	0.4	209.3	0.5	1.6
ZB1 (Z)	Z,Co,Clr,Eu,St,Abr,Dia	21	160	10	297	10	6	1058.6	0.11	0.2292	0.0005	0.033	0.00005	0.6313	209.3	0.6	209.5	0.9	1.3
ZB2 (Z)	Z,Co,Clr,Eu,Pr,Abr,Dia	9	215	63	175	6	15	1482.3	0.11	0.2289	0.0004	0.03294	0.00004	0.7560	208.9	0.4	209.3	0.7	2.0
ZB3 (Z)	Z,Co,Clr,Eu,St,Abr,Dia	37	118	50	214	7	3	6778.5	0.12	0.2290	0.0003	0.03295	0.00004	0.8774	209.0	0.5	209.4	0.5	2.6
06WX010A02 Guichon Phase, Guichon Batholith (Z9117) 10 642540E 5599029N UTM NAD83																			
ZA1 (Z)	Z,Co,Clr,Eq,Eu,Abr,Dia	1	230	36	173	6	8	1687.5	0.14	0.2326	0.0004	0.03333	0.00004	0.8519	211.3	0.5	212.3	0.7	5.4
ZA2 (Z)	Z,Co,Clr,Eu,Pr,Abr,Dia	3	220	49	174	6	6	2861.7	0.13	0.2332	0.0004	0.03354	0.00004	0.8890	212.6	0.5	212.9	0.6	1.2
ZA3 (Z)	Z,Co,Clr,Eq,Eu,Pr,Abr,Dl	4	213	50	119	4	3	3891.8	0.15	0.2316	0.0003	0.0333	0.00003	0.8711	211.2	0.4	211.5	0.5	2.1
ZB1 (Z)	Z,Co,Clr,Eu,St,Abr,Dia	4	225	35	119	4	1	3879.5	0.14	0.2315	0.0005	0.03332	0.00006	0.6980	211.3	0.8	211.5	0.8	1.0
ZD1 (Z)	Z,Co,Clr,Eq,Eu,Abr,Dia	1	250	20	68	2	3	933.1	0.15	0.2286	0.0008	0.03329	0.00004	0.5639	211.1	0.5	209.0	1.4	-14.0
06AT113A02 Bethlehem Phase, Guichon Batholith (Z9118) 10 643226E 5595450N UTM NAD83																			
ZB1 (Z)	Z,pBr,Clr,Eu,St,Abr,Dia	1	300	22	36	1	6	279.8	0.14	0.2301	0.0015	0.03312	0.00006	0.6397	210.1	0.8	210.3	2.5	1.1
ZB2 (Z)	Z,pBr,Clr,Eu,St,Abr,Dia	3	225	38	40	1	5	723.3	0.12	0.2303	0.0006	0.03315	0.00004	0.6878	210.3	0.5	210.5	1.0	1.3
ZB3 (Z)	Z,pBr,Clr,Eu,St,Abr,Dia	1	245	23	33	1	1	1648.1	0.13	0.2305	0.0005	0.03317	0.00003	0.6590	210.4	0.4	210.6	0.8	1.3
07WX024 Post-bethlehem Porphyry, Guichon Batholith (Z9377) 10 643335E 5595680N UTM NAD83																			
Z1A (Z)	Z,Co,Clr,Eq,Eu,Pr,Abr,Dl	2	200	69	88	3	4	2981.9	0.14	0.2298	0.0003	0.03309	0.00004	0.7445	209.8	0.5	210.1	0.6	1.4
Z2A (Z)	Z,Co,Clr,El,Eu,Pr,Abr,Dla	1	250	30	68	2	2	2349.3	0.14	0.2305	0.0004	0.03309	0.00003	0.7750	209.9	0.4	210.6	0.6	4.0
Z2B (Z)	Z,Co,Clr,Eu,Pr,Abr,Dia	2	250	61	71	2	3	2712.1	0.15	0.2310	0.0004	0.03321	0.00003	0.8143	210.6	0.4	211.0	0.6	2.2
Z3A (Z)	Z,Co,Clr,Eq,Eu,Pr,Abr,Dl	4	200	47	87	3	2	4392.3	0.14	0.2307	0.0003	0.03314	0.00003	0.8376	210.1	0.4	210.8	0.5	3.6

(1) Z=Zircon, Co=Colourless, pBr=Pale Brown, Clr=Clear, El=Elongate, Eq=Equant, Eu=Euhedral, Pr=Prismatic, St=Stubby Prism, Abr=Abraded, Dia = diamagnetic fractoin, M0° = magnetic at 0° sideslope.

(2) Concentration uncertainty varies with sample weight: >10% for sample weights <10 µg, <10% for sample weights above 10 µg.

(3) Pbr = radiogenic Pb. Pbc = total common Pb in analysis corrected for spike and fractionation.

(4) Atomic ratios corrected for spike, fractionation, blank and initial common Pb, except 206Pb/204Pb ratio corrected for spike and fractionation only. Errors are one sigma absolute. Pb blank 1-3 pg; blank composition (atomic proportions): 208Pb = 0.5197; 207Pb=0.2136; 206Pb=0.2529; 204Pb = 0.0139. Common Pb correction based on Stacey-Kramers (1975) model. U blank 0.1 pg; U fractionation calculated from double spike. Pb fractionation = 0.10±0.03% based on SRM981.

(5) Correlation coefficient of errors in isotopic ratios

do not define a single age population. The four youngest analyses have overlapping ages and yield a Concordia age of 215.55 ± 0.48 Ma (MSWD of concordance = 1.9; probability of concordance = 0.17; Table 1). The other two analyses have slightly older $^{206}Pb/^{238}U$ ages of 216.3 ± 0.5 Ma and 217.1 ± 0.6 Ma and are interpreted to be inherited. The best estimate of the crystallization age of the diorite is 215.55 ± 0.48 Ma.

Guichon phase (sample 06WX010A02): This Guichon phase sample was collected from a roadside outcrop north of Bethlehem pits on the Bose Lake road (Fig. 2). It is a homogeneous hornblende-biotite granodiorite with interstitial K-feldspar.

Zircon occurs as clear colorless euhedral prisms. Cathodoluminescence images reveal simple oscillatory zoned crystals, with no evidence for inherited cores (Fig. 5a). Four of five analyses of single to small, multi-grain fractions have overlapping $^{206}Pb/^{238}U$ ages at ~211.2 Ma, whereas the fifth analyses has a slightly older age of 212.6 Ma (Fig. 6b). A concordia age of 211.3 ± 0.7 Ma is calculated from the four younger fractions and is considered the best estimate of the crystallization age of the phase. The slightly older age of 212.6 Ma for fraction ZA2 indicates inheritance of a slightly older component, perhaps from the Border phase or other earlier intrusive unit. SHRIMP analyses (Table 2) of 19 zircon grains yield a single age population with a weighted mean $^{206}Pb/^{238}U$ age of 210 ± 2 Ma, within error of the TIMS age with no indication of a significantly older inherited component.

Table 2. U-Pb analytical data, SHRIMP ion microprobe

Spot	^{204}Pb/206Pb	±%	^{208}Pb/206Pb	±%	%^{206}Pbc	U ppm	Th ppm	^{232}Th/238U	206* ppm	^{207}Pbr/235U	±%	^{206}Pbr/238U	±%	error corr.	Age (Ma)	±
06WX010A02 Guichon Phase																
9117-1.1	1.8E-4	166	.188	3.8	0.34	178	96	0.56	5.14	0.2263	9.83	0.03354	1.17	.1190	212.6	2.4
9117-2.1	7.8E-4	35	.113	5.4	1.43	133	45	0.35	3.76	0.1941	10.89	0.03240	1.67	.1533	205.5	3.4
9117-3.1	1.2E-3	32	.191	4.2	2.25	150	65	0.45	4.26	0.2222	12.69	0.03233	1.36	.1069	205.1	2.7
9117-4.1	4.1E-5	232	.090	3.9	0.08	343	86	0.26	9.73	0.2346	4.83	0.03301	0.77	.1596	209.4	1.6
9117-7.1	1.6E-4	213	.147	6.0	0.29	87	37	0.44	2.51	0.2263	11.14	0.03372	1.56	.1400	213.8	3.3
9117-10.1	5.9E-4	65	.141	6.3	1.09	90	34	0.38	2.48	0.1885	14.45	0.03162	1.62	.1121	200.7	3.2
9117-8.1	1.0E-5	2	.145	6.7	0.02	92	35	0.39	2.64	0.2599	4.27	0.03342	1.40	.3287	211.9	2.9
9117-9.1	4.2E-4	32	.167	3.6	0.77	205	100	0.50	5.89	0.1975	5.70	0.03321	0.95	.1674	210.6	2.0
9117-12.1	2.7E-4	50	.116	4.6	0.49	196	67	0.36	5.53	0.2158	5.32	0.03274	1.01	.1898	207.7	2.1
9117-13.1	2.1E-5	300	.146	2.6	0.04	419	181	0.45	12.1	0.2322	2.72	0.03355	0.64	.2371	212.7	1.3
9117-14.1	4.5E-4	42	.194	3.6	0.82	198	106	0.55	5.64	0.2055	7.14	0.03294	1.03	.1447	208.9	2.1
9117-26.1	3.3E-4	57	.192	3.4	0.60	221	122	0.57	6.36	0.2190	6.67	0.03332	0.98	.1471	211.3	2.0
9117-24.1	3.1E-4	51	.190	3.5	0.58	209	113	0.56	5.9	0.2080	6.14	0.03269	0.99	.1619	207.3	2.0
9117-20.1	1.9E-4	207	.146	6.2	0.34	75	30	0.41	2.13	0.2163	12.92	0.03269	1.65	.1276	207.4	3.4
9117-39.1	1.0E-5	1	.187	4.5	0.02	130	74	0.59	3.68	0.2305	3.82	0.03298	1.19	.3127	209.2	2.5
9117-40.1	8.0E-5	120	.142	3.3	0.15	307	126	0.42	8.74	0.2345	3.73	0.03305	1.07	.2858	209.6	2.2
9117-41.1	1.2E-3	30	.162	5.0	2.29	103	53	0.53	3.03	0.1637	17.56	0.03352	1.47	.0834	212.6	3.1
9117-42.1	3.7E-4	66	.105	6.7	0.68	115	35	0.32	3.28	0.2192	8.62	0.03289	1.32	.1526	208.6	2.7
9117-43.1	3.1E-4	82	.134	5.2	0.57	126	51	0.42	3.56	0.2149	9.10	0.03270	1.77	.1946	207.4	3.6
06AT113A02 Bethlehem Phase																
9118-55.1	6.1E-5	121	.088	5.5	0.11	149	35	0.25	4.3	0.2492	4.22	0.03359	2.21	.5229	213.0	4.6
9118-57.1	1.6E-4	356	.126	14.3	0.29	24	6	0.28	0.665	0.2348	18.35	0.03165	5.12	.2793	200.9	10.1
9118-58.1	4.0E-4	97	.124	5.8	0.74	107	33	0.32	3	0.2152	12.80	0.03236	1.47	.1147	205.3	3.0
9118-2.1	5.1E-4	32	.188	5.1	0.94	87	46	0.55	2.48	0.2183	6.98	0.03292	1.40	.2012	208.8	2.9
9118-8.1	1.0E-5	65	.112	5.7	0.02	141	43	0.32	3.98	0.2278	3.60	0.03289	1.14	.3167	208.6	2.3
9118-9.1	1.0E-5	48	.098	6.3	0.02	108	30	0.28	3.07	0.2473	3.78	0.03299	1.24	.3286	209.3	2.6
9118-13.1	1.0E-5	2	.099	7.8	0.02	74	17	0.24	2.13	0.2456	4.67	0.03351	1.51	.3239	212.5	3.2
9118-17.1	3.7E-4	33	.148	3.0	0.68	310	132	0.44	9	0.2087	4.84	0.03356	0.78	.1602	212.8	1.6
9118-19.1	4.2E-4	32	.135	5.0	0.76	134	50	0.39	3.83	0.2205	5.87	0.03298	1.83	.3124	209.2	3.8
9118-26.1	4.5E-4	52	.132	4.6	0.82	151	54	0.37	4.34	0.2150	8.25	0.03309	1.13	.1367	209.9	2.3
9118-27.1	1.0E-5	45	.158	7.2	0.02	57	23	0.42	1.64	0.2332	5.46	0.03310	1.76	.3226	209.9	3.6
9118-28.1	3.6E-4	3	.140	4.9	0.67	126	57	0.47	3.63	0.2189	3.93	0.03342	1.14	.2913	211.9	2.4
9118-25.1	7.7E-4	19	.100	6.7	1.41	104	29	0.29	2.97	0.1768	8.03	0.03283	1.75	.2177	208.2	3.6
9118-23.1	1.0E-3	37	.145	7.6	1.92	48	20	0.43	1.43	0.1834	16.84	0.03400	1.96	.1164	215.5	4.2
06WX04A01 Bethsaida Phase																
9116-3.1	4.4E-4	60	.092	5.9	0.81	148	38	0.26	4.2	0.2091	9.47	0.03285	1.23	.1302	208.4	2.5
9116-23.1	1.0E-5	56	.097	4.6	0.02	235	63	0.27	6.63	0.2345	2.79	0.03285	0.90	.3205	208.4	1.8
9116-44.1	3.7E-4	68	.102	5.2	0.69	167	48	0.30	4.75	0.2143	8.72	0.03283	1.15	.1318	208.3	2.4
9116-7.1	1.0E-5	60	.113	5.5	0.02	167	58	0.36	4.78	0.2362	3.34	0.03333	1.06	.3179	211.3	2.2
9116-28.1	2.6E-4	59	.103	7.0	0.48	137	43	0.32	3.93	0.2204	6.26	0.03309	1.73	.2757	209.8	3.6
9116-48.1	3.5E-4	73	.063	10.6	0.64	74	13	0.18	2.1	0.2007	10.02	0.03274	1.64	.1635	207.7	3.3
9116-48.2	2.4E-4	160	.110	4.8	0.44	191	65	0.35	5.29	0.2148	12.23	0.03217	1.21	.0992	204.1	2.4
9116-50.1	1.0E-5	53	.098	5.3	0.02	169	47	0.29	4.77	0.2398	3.24	0.03283	1.03	.3194	208.3	2.1
9116-51.1	7.4E-4	19	.117	6.9	1.36	77	23	0.31	2.18	0.1906	7.62	0.03246	1.54	.2024	205.9	3.1
06AT113A01 Gnawed Mountain Porphyry																
9115-2.1	1.0E-5	51	.080	5.0	0.02	228	56	0.26	6.68	0.2377	2.85	0.03404	0.99	.3479	215.8	2.1
9115-4.1	1.0E-5	1	.103	4.1	0.02	286	84	0.30	7.87	0.2230	2.64	0.03196	0.91	.3461	202.8	1.8
9115-4.2	1.5E-4	70	.084	4.6	0.27	278	68	0.25	7.88	0.2219	4.16	0.03283	0.86	.2057	208.2	1.8
9115-8.1	3.4E-4	45	.078	5.2	0.63	225	43	0.20	6.32	0.2054	5.94	0.03250	0.96	.1619	206.2	2.0
9115-8.2	1.3E-4	81	.077	6.8	0.23	239	53	0.23	6.32	0.2131	5.20	0.03072	1.21	.2330	~~195.0~~	~~2.3~~
9115-10.1	2.2E-4	22	.055	6.4	0.41	201	36	0.18	5.7	0.2196	3.60	0.03284	1.27	.3539	208.3	2.6
9115-10.2	3.2E-4	69	.057	6.1	0.59	213	36	0.17	5.97	0.2051	7.88	0.03243	1.01	.1280	205.8	2.0
9115-11.1	1.0E-5	69	.072	4.8	0.02	300	58	0.20	8.54	0.2380	2.51	0.03313	0.81	.3231	210.1	1.7
9115-12.1	1.0E-5	52	.072	5.6	0.02	214	42	0.20	5.96	0.2281	3.13	0.03249	1.31	.4179	206.1	2.7
9115-14.1	2.9E-4	71	.074	5.4	0.54	218	44	0.21	6.04	0.2106	7.20	0.03206	1.01	.1397	203.4	2.0
9115-18.1	8.9E-5	50	.060	5.7	0.16	223	40	0.18	6.23	0.2116	3.22	0.03251	0.89	.2770	206.2	1.8
9115-19.1	6.4E-4	5	.064	5.4	1.17	260	48	0.19	7.2	0.1873	3.63	0.03185	0.87	.2387	202.1	1.7
9115-19.2	3.5E-4	31	.081	5.2	0.64	222	56	0.26	6.31	0.2088	4.78	0.03282	0.97	.2038	208.2	2.0
9115-24.1	3.4E-5	395	.077	6.2	0.06	151	35	0.24	4.61	0.2593	4.99	0.03547	1.35	.2714	~~224.7~~	~~3.0~~
9115-21.1	1.0E-5	63	.104	4.6	0.02	267	77	0.30	7.53	0.2333	2.67	0.03279	0.85	.3187	208.0	1.7
9115-26.1	1.0E-5	48	.073	5.6	0.02	223	47	0.22	6.25	0.2360	3.70	0.03258	0.92	.2500	206.7	1.9
9115-28.1	2.3E-4	53	.065	5.1	0.42	274	54	0.21	7.76	0.2116	5.61	0.03287	0.85	.1523	208.5	1.8
9115-28.2	1.0E-5	156	.077	4.9	0.02	261	57	0.23	7.37	0.2266	2.70	0.03285	0.85	.3148	208.3	1.7
9115-29.1	7.8E-4	81	.043	5.6	1.43	358	44	0.13	10.3	0.1743	25.27	0.03310	1.39	.0549	209.9	2.9
9115-31.1	1.0E-4	130	.064	5.9	0.19	215	40	0.19	5.96	0.2153	5.07	0.03221	0.97	.1905	204.3	1.9
9115-32.1	2.0E-4	56	.091	3.9	0.36	344	91	0.27	9.73	0.2180	4.23	0.03284	1.05	.2487	208.3	2.2

Spot name follows the convention x-y.z; where x = sample number, y = grain number and z = spot number.
Uncertainties are 1-sigma; Pb$_c$ and Pb* indicate the common and radiogenic portions, respectively.
%^{206}Pbc refers to mole fraction of total ^{206}Pb that is due to common Pb, calculated using the 204Pb-method; common Pb composition used is the surface blank (4/6: 0.05770; 7/6: 0.89500; 8/6: 2.13840)
Calibration standard 6266; U = 910 ppm; Age = 559 Ma; 206Pb/238U = 0.09059; Pb/U calibration includes a quadratically added uncertainty of 0.8%
Uncertainty in Standard calibration was 0.11% (not included in above errors but required when comparing data from different mounts; or different methods).

Bethlehem Suite

Bethlehem phase (sample 06AT113A02): This sample was collected from the Bethlehem phase within the Jersey pit of the Bethlehem deposit. The sample is a hornblende-biotite granodiorite, similar to the phase that hosts mineralization within the pit, although the geochronology sample is not mineralized.

Zircon occurs as euhedral prisms with broad oscillatory zoning (Fig. 5b). Two single grain and one multiple grain (3) analyses yield overlapping concordant results with a concordia age of 210.3 ± 0.4 Ma (Fig. 6c). SHRIMP analyses of fourteen grains yields a similar age of 210.4 ± 2 Ma and do not indicate a significantly older component in any of the zircon.

Post-mineralization dyke, Bethlehem deposit (sample 07WX024): This white, densely-packed, feldspar-quartz-amphibole porphyry dyke sample, is from one of a swarm of dykes identified by McMillan (1985)

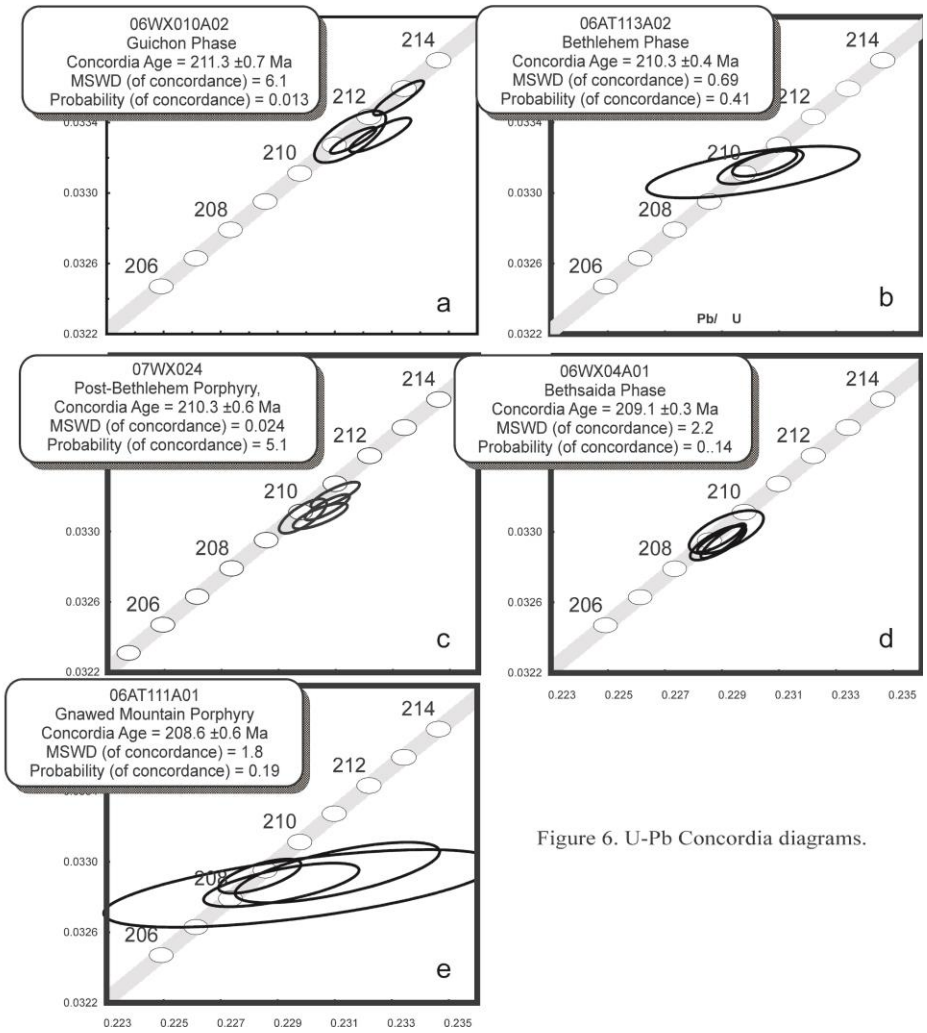

Figure 6. U-Pb Concordia diagrams.

as post-dating mineralization at Bethlehem deposit. It was collected from the south wall of the now closed Jersey open pit. In outcrop, this moderately altered but barren dyke clearly post-dates mineralization, as it cross-cuts strongly altered and sulfide-fracture-bearing Bethlehem phase rocks (Fig. 7). The ragged amphibole in the sample is feldspar-poikiolitic and texturally resembles the host Bethlehem phase. Based on its major element composition, this sample is a calcic tonalite (Fig. 3), due to post-mineralization

secondary calcite alteration, which is also evidenced by a 'bleached' white appearance and chlorite plus epidote alteration of amphibole. Over six years after this dated dyke sample was collected, a detailing study was carried out of Bethlehem deposit felsic dyke rocks and their associated alteration by Byme et al. (2017). In their study, they noted the importance of strongly metasomatic Na-Ca alteration of post-

Figure 7. Photograph of sample site of post-mineralization dyke cutting altered Bethlehem phase host rock.

mineralization dykes within the Bethleham deposit. For this reason, our two dyke samples were not utilized in geochemical modeling or petrogenetic discussion that were carried out in this study.

Zircon consists of euhedral prismatic crystals with well-developed oscillatory and sector zoning (Fig. 5c). Four analyses consisting of one to four grains yield overlapping, concordant results which provide a concordia age of 210.3 ± 0.6 Ma (Fig. 6d). The age is identical to that from the host Bethlehem phase granodiorite, indicating that the two phases were intruded within 1 Ma of each other. The age of the dyke also indicates that fracture-related mineralization plus accompanying alteration in the Bethlehem deposit occurred during the interval between intrusion of the host and dyke phases. Post-dyke alteration of the Bethlehem deposit is probably related to alteration associated with the proximal (3-6 km) Bethsaida phase which hosts the Valley JA and Valley deposits.

Bethsaida phase (sample 06WX04A01): The Bethsaida phase sample was collected from a roadcut on the Calling Lake road, southwest of the Lornex pit (Fig. 2). The sample is a quartz-biotite porphyritic granodiorite, similar to mineralized phases of the pluton observed in the Lornex and Valley pits.

Zircon occurs as euhedral prismatic grains with well-developed oscillatory zoning and no evidence for inherited cores (Fig. 5d). Five of six analyses, ranging from 8 to 37 grains each, yield overlapping concordant results with a concordia age of 209.1 ± 0.3 Ma (Fig. 6e). This is interpreted to be the crystallization age for the Bethsaida phase. A single analysis has an older $^{206}Pb/^{238}$ age of ~216 Ma and may

indicate an older component in this fraction. The TIMS age is supported by nine SHRIMP analyses that yielded a weighted mean $^{206}Pb/^{238}U$ age of 208 ± 2 Ma, but did not indicate an obvious inherited component.

Gnawed Mountain subphase (sample 06AT111A01): The Gnawed Mountain subphase sample was collected from a dyke within the Highmont pit. This subphase, consisting of biotite-quartz-feldspar porphyry, is, based on field relationships, one of the youngest intrusive phases in the area and cross-cuts the Skeena phase within the pit. McMillan (1985) associated it with the Bethsaida phase and, as portions are mineralized and locally attain ore grades, interpreted it as having intruded late in the mineralization process.

Zircon occurs as euhedral, finely oscillatory zoned crystals without evidence for cores (Fig. 5e). Four analyses consisting of between 4 and 12 grains yield overlapping concordant ages with a concordia age of 208.6 ± 0.6 Ma (Fig. 6f) interpreted as the crystallization age of the dyke. SHRIMP analyses of 20 individual grains yield a dominant population with a weighted mean $^{206}Pb/^{238}$ age of 207 ± 2 Ma. Two analyses yielded significantly older ages of 216 and 225 Ma, indicating inheritance of zircon from a slightly older source, perhaps part of the Upper Triassic Nicola Group volcanic host rocks.

Ar-Ar Geochronology

Analytical techniques

Selected samples were processed for $^{40}Ar/^{39}Ar$ analysis of whole rock by standard preparation techniques, including hand-picking of unaltered pieces in the size range 0.25 to 0.50 mm. Individual mineral separates were loaded into aluminum foil packets along with a single grain of Fish Canyon Tuff Sanidine (FCT-SAN) to act as flux monitor (apparent age = 28.03 Ma; Renne et al., 1994). The sample packets were arranged radially inside an aluminum can. The samples were then irradiated for 12 hours at the research reactor of McMaster University in a fast neutron flux of approximately $3x10^{16}$ neutrons/cm^2.

Laser $^{40}Ar/^{39}Ar$ step-heating analysis was carried out at the Geological Survey of Canada laboratories in Ottawa, Ontario. Upon return from the reactor, samples were split into several aliquots and loaded into individual 1.5 mm-diameter holes in a copper planchet. The planchet was then placed in the extraction line and the system evacuated. Heating of individual sample aliquots in steps of increasing temperature was achieved using a Merchantek MIR10 10W CO_2 laser equipped with a 2 mm x 2 mm flat-field lens. The released Ar gas was cleaned over getters for ten minutes, and then analyzed isotopically using the secondary electron multiplier system of a VG3600 gas source mass spectrometer; details of data

collection protocols can be found in Villeneuve and MacIntyre (1997) and Villeneuve et al. (2000). Error analysis on individual steps follows numerical error analysis routines outlined in Scaillet (2000); error analysis on grouped data follows algebraic methods of Roddick (1988).

Corrected argon isotopic data are listed in Table 2, and presented (Fig. 2 and 3) as spectra of gas release or on inverse-isochron plots (Roddick et al. 1980). Each gas-release spectrum plotted contains step-heating data from up to two aliquots, alternately shaded and normalized to the total volume of ^{39}Ar released for each aliquot. Such plots provide a visual image of replicated heating profiles, evidence for Ar-loss in the low temperature steps, and the error and apparent age of each step.

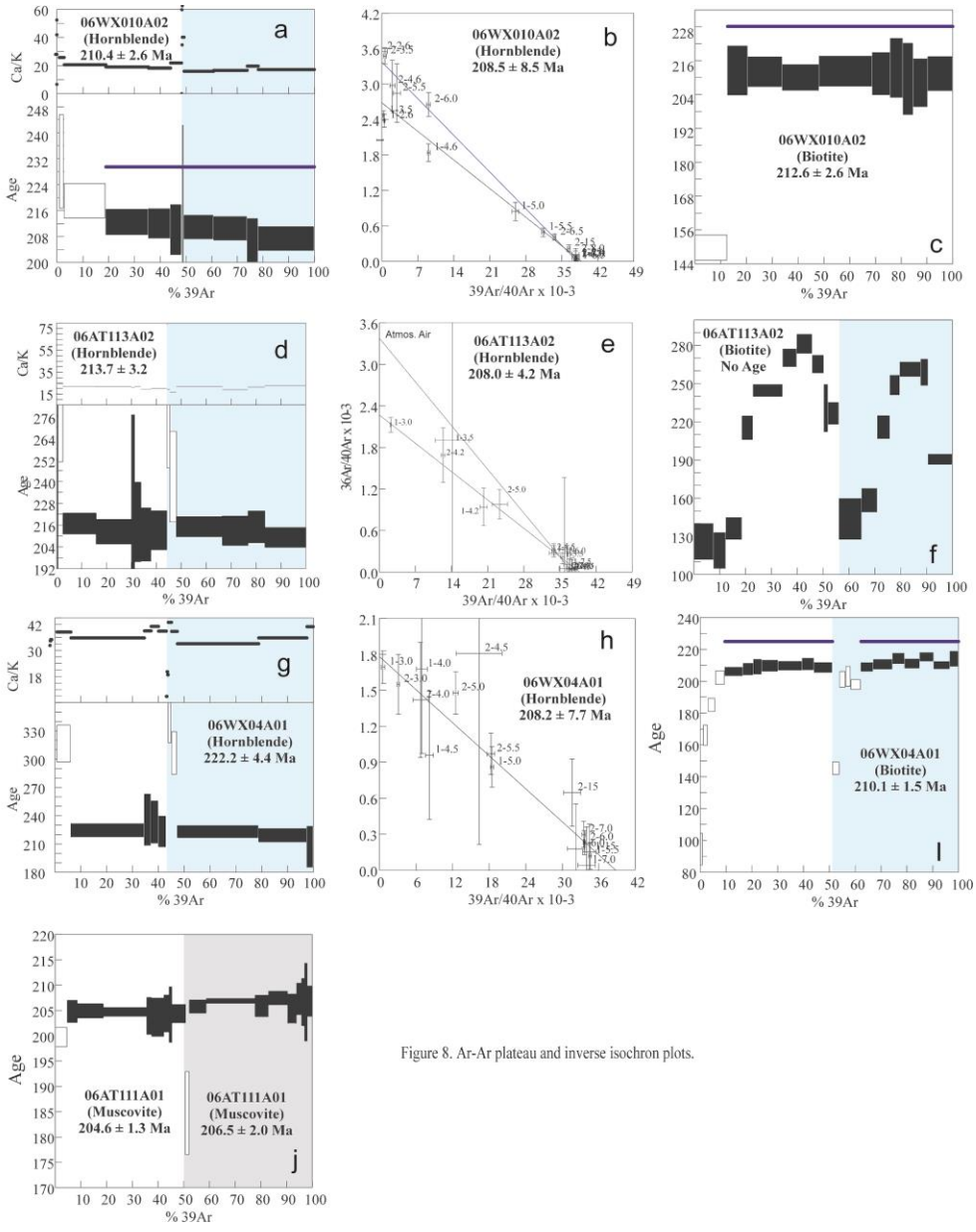

Figure 8. Ar-Ar plateau and inverse isochron plots.

Table 3. CO_2 laser step-heating $^{40}Ar/^{39}Ar$ data[e,f,g]. All uncertainties quoted at 2s level.

Power[a]	Volume ^{39}Ar x10^{-11} cc	$^{36}Ar/39Ar$	±	$^{37}Ar/39Ar$	±	$^{38}Ar/39Ar$	±	$^{40}Ar/39Ar$	±	%^{40}Ar ATM	$^{40*}Ar/^{39}Ar$	±	f_{39}[b] (%)	Apparent Age Ma[c]	±
06WX010A02 Hornblende; J=.00474430 Guichon Phase, Guichon Batholith (Z9117)															
Aliquot: A															
2.6	0.0104	4.8419	0.9651	3.475	10.420	7.357	1.496	2033.02	394.83	70.4	602.25	135.15	0.1	2435.5	300.6
3.5	0.006	7.3431	3.4514	27.247	21.940	7.949	3.745	2977.13	1396.78	72.9	807.24	385.52	0	2841.1	696.8
4.2	0.018	1.7307	0.3044	21.802	7.891	2.843	0.482	607.82	95.88	84.1	96.38	44.65	0.1	679.4	262.7
4.6	0.0822	0.2028	0.0164	14.582	1.473	2.891	0.112	110.15	3.32	54.4	50.21	5.30	0.5	385.5	36.7
5	0.2868	0.0325	0.0060	13.405	0.641	1.717	0.040	38.49	0.98	25	28.88	1.97	1.9	231.7	14.8
5.5	2.4692	0.0157	0.0023	10.729	0.268	1.735	0.019	31.87	0.28	14.5	27.25	0.73	16.2	219.3	5.5
6	2.5316	0.0007	0.0017	9.902	0.254	1.601	0.017	26.58	0.16	0.8	26.37	0.54	16.6	212.6	4.1
6.5	1.3057	0.0002	0.0019	9.476	0.309	1.594	0.022	26.37	0.24	0.3	26.30	0.62	8.6	212.2	4.7
15	0.6602	0.0016	0.0031	11.380	0.415	1.729	0.034	26.52	0.52	1.8	26.05	1.04	4.3	210.2	8.0
Aliquot: B															
2.6	-0.0001	-49.0507	-784.5931	-2961.675	-47505.270	-70.349	-1125.225	-13826.24	221112.44	104.8	668.25	11922.95	0	2576.3	11880.4
3.5	0.0099	5.9485	2.8137	83.300	65.937	4.441	2.148	1710.28	806.38	102.8	-47.49	-73.18	0.1	-460.5	825.0
4.2	0.0092	3.9977	1.1449	31.041	40.252	7.038	1.991	1358.66	382.95	86.9	177.33	80.62	0.1	1101.3	376.7
4.6	0.0069	1.4624	0.3975	18.065	58.290	2.857	0.823	491.04	116.62	88	58.89	64.62	0.1	444.5	433.7
5	0.0091	1.0873	0.3598	78.291	51.575	2.645	0.605	186.57	39.68	172.2	-134.74	-90.49	0.1	-1839.3	2375.8
5.5	0.0077	0.9702	0.2757	32.535	51.602	5.013	1.215	340.68	80.49	84.2	53.99	52.45	0.1	411.4	358.4
6	0.1019	0.2914	0.0247	20.912	4.711	2.484	0.124	109.75	4.52	78.5	23.64	6.67	0.7	191.8	51.3
6.5	1.7538	0.0122	0.0016	8.332	0.367	1.570	0.034	29.76	0.19	12.1	26.15	0.50	11.5	211.0	3.8
7	1.9912	0.0011	0.0016	8.649	0.404	1.370	0.017	26.44	0.18	1.3	26.10	0.51	13.1	210.6	3.9
8	0.6573	0.0031	0.0027	10.174	1.079	1.339	0.030	26.52	0.49	3.5	25.60	0.93	4.3	206.8	7.1
15	3.3232	0.0061	0.0016	8.951	0.372	1.595	0.017	27.48	0.19	6.5	25.68	0.50	21.8	207.4	3.9
06WX010A02 Biotite; J=.00427060 Guichon Phase, Guichon Batholith (Z9117)															
Aliquot: A															
3	2.5217	0.0121	0.0016	0.110	0.007	0.207	0.014	23.85	0.50	15	20.26	0.67	12.6	149.7	4.7
3.5	1.5855	0.0019	0.0028	0.061	0.008	0.218	0.015	30.03	1.05	1.8	29.48	1.32	7.9	213.9	9.0
4	2.6666	0.0015	0.0014	0.036	0.007	0.243	0.015	29.86	0.70	1.5	29.41	0.81	13.3	213.4	5.5
4.5	2.8667	0.0014	0.0015	0.057	0.006	0.217	0.013	29.53	0.56	1.4	29.11	0.70	14.3	211.4	4.8
5	4.1225	0.0010	0.0010	0.099	0.006	0.238	0.014	29.75	0.77	1	29.44	0.82	20.6	213.6	5.6
5.5	1.3952	0.0033	0.0026	0.079	0.012	0.199	0.014	30.29	0.86	3.3	29.31	1.14	7	212.7	7.8
6	0.9809	0.0029	0.0038	0.150	0.011	0.257	0.019	30.48	1.12	2.8	29.62	1.58	4.9	214.9	10.8
7.5	1.1184	0.0022	0.0027	0.069	0.010	0.253	0.032	29.49	1.02	2.2	28.83	1.28	5.6	209.5	8.8
6.5	0.8098	0.0020	0.0046	0.072	0.020	0.221	0.019	29.63	1.33	2	29.03	1.90	4.1	210.9	13.0
15	1.9269	0.0007	0.0017	0.052	0.007	0.227	0.017	29.51	0.77	0.7	29.31	0.92	9.6	212.8	6.3
06AT113A02 Hornblende; J=.00474530Bethlehem Phase, Guichon Batholith (Z9118; 0.0000-N 0.0000-E)															
Aliquot: A															
3	0.0311	0.9504	0.0640	8.066	3.293	4.427	0.247	446.85	22.41	62.8	166.01	16.92	0.4	1048.1	81.1
3.5	0.0168	0.1344	0.1386	5.466	6.113	1.513	0.240	70.63	16.30	56.2	30.92	42.66	0.2	247.0	319.0
4.2	0.1522	0.0465	0.0133	12.527	0.892	1.661	0.052	49.44	1.70	27.8	35.70	4.23	2	282.3	31.0
5	1.0326	0.0089	0.0024	11.360	0.364	1.599	0.022	29.57	0.31	8.8	26.95	0.77	13.3	217.1	5.8
5.5	1.1024	0.0063	0.0029	11.159	0.326	1.609	0.021	28.22	0.29	6.6	26.36	0.90	14.2	212.6	6.9
6	0.0931	0.0077	0.0303	10.785	1.218	1.552	0.069	27.89	2.24	8.1	25.63	9.24	1.2	207.0	70.5
6.5	0.1987	0.0015	0.0090	11.331	0.816	1.501	0.049	27.50	1.15	1.6	27.07	2.91	2.6	218.0	22.1
7.5	0.3089	0.0031	0.0058	10.019	0.661	1.485	0.047	27.06	0.90	3.4	26.15	1.94	4	211.0	14.8
15	0.4939	0.0010	0.0045	10.279	0.479	1.480	0.025	26.76	0.52	1.1	26.46	1.43	6.4	213.4	10.9
Aliquot: B															
3	0.0153	1.2636	0.1703	40.413	30.439	3.026	0.369	447.15	46.68	83.5	73.76	35.50	0.2	541.5	225.3
4.2	0.0836	0.1363	0.0316	9.945	4.322	0.565	0.021	80.71	2.33	49.9	40.43	9.54	1.1	316.6	68.5
5	0.2011	0.0419	0.0094	8.679	2.021	0.481	0.040	42.81	2.74	29	30.42	3.36	2.6	243.2	25.2
5.5	1.4341	0.0097	0.0024	11.206	0.555	1.486	0.019	29.59	0.24	9.7	26.72	0.74	18.5	215.4	5.6
6	0.7978	0.0012	0.0035	9.717	0.754	1.352	0.023	26.79	0.30	1.4	26.43	1.07	10.3	213.1	8.1
7	0.5246	0.0015	0.0037	11.032	1.032	0.864	0.020	27.16	0.43	1.7	26.71	1.16	6.8	215.3	8.9
15	1.2753	0.0013	0.0023	11.559	0.526	0.877	0.015	26.33	0.23	1.5	25.94	0.72	16.4	209.5	5.5
06AT113A02 Biotite; J=.00427250 Bethlehem Phase, Guichon Batholith (Z9118)															
Aliquot: A															
3	2.6589	0.4248	0.0104	1.999	0.066	0.359	0.017	142.40	3.51	88.1	16.88	2.00	7.6	125.6	14.4
3.5	1.6582	0.1901	0.0090	1.672	0.068	0.298	0.018	72.07	2.60	77.9	15.90	1.98	4.8	118.6	14.3
4	2.169	0.1383	0.0043	1.433	0.045	0.287	0.014	59.18	1.10	69.1	18.31	1.24	6.2	135.9	8.9
4.5	1.5082	0.0275	0.0036	1.293	0.069	0.368	0.021	37.74	1.06	21.5	29.62	1.40	4.3	215.0	9.5
5	4.0059	0.0207	0.0012	1.227	0.061	0.388	0.017	40.06	0.76	15.3	33.94	0.73	11.5	244.3	4.9
5.5	1.8862	0.0178	0.0020	0.909	0.045	0.401	0.018	43.04	1.01	12.2	37.77	1.08	5.4	269.9	7.2
6	2.0883	0.0204	0.0024	1.615	0.080	0.442	0.025	45.47	1.06	13.3	39.44	1.18	6	280.9	7.8
6.5	1.5687	0.0208	0.0021	1.927	0.133	0.339	0.015	43.18	1.00	14.2	37.03	1.08	4.5	265.0	7.2
7.5	0.5689	0.0290	0.0062	5.514	0.358	0.252	0.036	40.46	2.43	21.2	31.88	2.77	1.6	230.4	18.8
15	1.4714	0.0259	0.0028	4.082	0.163	0.150	0.014	38.95	1.22	19.7	31.28	1.31	4.2	226.3	8.9
Aliquot: B															
3	3.0655	0.4267	0.0120	1.716	0.068	0.262	0.025	145.45	3.23	86.7	19.36	2.29	8.8	143.4	16.3
3.5	2.1073	0.1060	0.0045	1.286	0.148	0.247	0.013	52.74	0.99	59.4	21.43	1.35	6	158.0	9.5
4	1.7112	0.0274	0.0033	1.013	0.074	0.280	0.024	37.80	1.17	21.4	29.70	1.35	4.9	215.5	9.2
4.5	1.3235	0.0243	0.0024	1.173	0.076	0.307	0.021	41.76	1.10	17.2	34.57	1.18	3.8	248.5	7.9
5	2.8336	0.0228	0.0021	1.228	0.093	0.306	0.016	43.16	0.74	15.6	36.42	0.89	8.1	260.9	5.9
6	0.9861	0.0115	0.0035	2.282	0.189	0.209	0.022	39.46	1.28	8.6	36.07	1.58	2.8	258.6	10.6
15	3.2617	0.0087	0.0015	1.961	0.094	0.044	0.011	28.60	0.47	9	26.03	0.62	9.4	190.2	4.3
06WX04A01 Hornblende; J=.00474330Bethsaida Phase, Guichon Batholith (Z9116; 0.0000-N 0.0000-E)															
Aliquot: A															
3	0.0109	2.5988	0.7401	16.791	9.327	2.169	0.659	1534.89	420.81	50	766.95	219.62	0.1	2768.0	407.8
4	0.0211	0.2419	0.1029	17.900	4.593	0.297	0.066	144.24	18.54	49.6	72.77	32.57	0.2	535.0	207.4
4.5	0.033	0.1174	0.0654	18.207	2.820	0.361	0.042	122.43	9.92	28.3	87.75	21.14	0.4	627.8	127.8
5	0.4685	0.0466	0.0092	20.011	0.729	0.303	0.014	54.16	0.83	25.4	40.40	2.79	5.4	316.3	20.1
5.5	2.4555	0.0034	0.0032	18.596	0.379	0.285	0.011	28.91	0.17	3.5	27.90	0.97	28.4	224.2	7.4
6	0.2262	0.0055	0.0116	20.296	0.892	0.332	0.018	31.02	1.33	5.3	29.39	3.67	2.6	235.4	27.6
7	0.2511	0.0012	0.0094	21.368	1.103	0.223	0.014	29.40	1.22	1.2	29.05	3.03	2.9	232.9	22.8
15	0.2584	0.0044	0.0068	20.234	0.728	0.199	0.013	29.02	0.93	4.5	27.72	2.21	3	222.8	16.7
Aliquot: B															
3	0.0217	0.5078	0.0861	4.608	5.054	0.828	0.073	327.65	21.61	45.8	177.60	27.64	0.3	1102.4	128.4
4	0.0242	0.2118	0.0802	10.506	5.117	0.295	0.076	149.24	28.01	41.9	86.66	27.30	0.3	621.2	166.1
4.5	0.0181	0.1106	0.0968	9.793	6.170	0.071	0.051	61.17	14.10	53.4	28.50	30.55	0.2	228.7	230.5
5	0.1105	0.1184	0.0143	22.324	1.665	0.338	0.027	80.01	2.82	43.7	45.03	4.65	1.3	349.2	32.8
5.5	0.196	0.0530	0.0095	20.165	1.094	0.297	0.020	54.64	1.90	28.6	38.98	3.18	2.3	306.1	23.0
6	2.7215	0.0068	0.0030	17.205	0.384	0.285	0.011	29.71	0.18	6.7	27.71	0.90	31.5	222.8	6.8
7	1.6168	0.0089	0.0033	18.619	0.448	0.254	0.012	29.82	0.23	8.8	27.19	0.99	18.7	218.9	7.5
15	0.2109	0.0204	0.0089	21.284	1.184	0.196	0.014	31.62	1.37	19.1	25.58	2.90	2.4	206.6	22.1
06WX04A01 Biotite; J=.00426870 Bethsaida Phase, Guichon Batholith (Z9116)															
Aliquot: A															
3	1.0357	0.0294	0.0038	0.530	0.037	0.025	0.011	21.24	0.95	40.8	12.57	1.39	1.2	94.3	10.2
3.5	1.6875	0.0076	0.0023	0.113	0.011	0.015	0.011	24.80	0.67	9	22.56	0.94	1.9	165.9	6.6
3.9	2.4899	0.0056	0.0014	0.080	0.009	0.017	0.011	26.93	0.50	6.1	25.28	0.64	2.9	184.9	4.4
4.5	3.1197	0.0023	0.0014	0.036	0.006	0.016	0.011	28.45	0.52	2.4	27.76	0.65	3.6	202.0	4.5
5	6.1924	0.0017	0.0008	0.063	0.005	0.016	0.011	28.82	0.34	1.7	28.32	0.42	7.1	205.9	2.9
5.5	3.5524	0.0023	0.0012	0.058	0.008	0.017	0.011	29.24	0.43	2.4	28.54	0.56	4.1	207.4	3.8
6	2.823	0.0008	0.0016	0.060	0.009	0.026	0.011	29.00	0.52	0.8	28.76	0.71	3.2	208.9	4.8

6.5	5.5139	0.0016	0.0008	0.103	0.010	0.019	0.011	29.33	0.49	1.6	28.85	0.53	6.3	209.5	3.7
7	8.092	0.0017	0.0006	0.101	0.007	0.018	0.011	29.36	0.40	1.7	28.85	0.43	9.3	209.5	2.9
8	4.0483	0.0016	0.0011	0.213	0.017	0.017	0.011	29.48	0.46	1.6	29.01	0.56	4.6	210.6	3.8
15	6.1538	0.0088	0.0007	0.093	0.005	0.027	0.011	31.29	0.46	8.3	28.69	0.48	7.1	208.4	3.3
Aliquot: B															
3	2.4616	0.0098	0.0013	0.116	0.026	0.011	0.011	22.53	0.51	12.9	19.63	0.60	2.8	145.1	4.2
3.5	2.0343	0.0017	0.0017	0.001	0.008	0.009	0.011	28.10	0.56	1.8	27.60	0.75	2.3	200.9	5.2
4	1.7602	0.0028	0.0017	0.002	0.005	0.015	0.011	28.69	0.80	2.8	27.87	0.93	2	202.8	6.4
4.5	3.3804	0.0027	0.0008	0.002	0.006	0.014	0.011	27.93	0.44	2.9	27.13	0.49	3.9	197.7	3.4
5	4.1815	0.0007	0.0008	0.051	0.017	0.014	0.011	28.94	0.34	0.7	28.74	0.42	4.8	208.7	2.9
5.5	6.5414	0.0012	0.0013	0.024	0.009	0.015	0.011	29.34	0.28	1.2	28.98	0.47	7.5	210.4	3.2
6	4.1104	0.0009	0.0009	0.019	0.003	0.016	0.011	29.79	0.45	0.9	29.52	0.52	4.7	214.1	3.5
6.5	5.0667	0.0002	0.0004	0.031	0.009	0.014	0.011	29.11	0.44	0.2	29.05	0.45	5.8	210.9	3.1
7	4.7392	0.0008	0.0006	0.073	0.011	0.016	0.011	29.90	0.38	0.8	29.66	0.42	5.4	215.1	2.9
8	5.478	0.0006	0.0006	0.121	0.008	0.015	0.011	29.06	0.33	0.6	28.90	0.36	6.3	209.9	2.5
15	2.8262	0.0006	0.0010	0.017	0.017	0.014	0.011	29.66	0.66	0.6	29.49	0.72	3.2	213.9	4.9
06AT111A01 Muscovite; J=.00474230 Gnawed Mountain Porphyry (Z9115)															
Aliquot: A															
2.4	1.2707	0.0097	0.0034	0.288	0.055	0.000	0.011	25.57	0.36	11.2	22.70	1.07	3.2	184.5	8.3
2.8	5.3802	0.0011	0.0005	0.055	0.011	0.001	0.011	25.75	0.10	1.2	25.44	0.18	13.4	205.5	1.4
3	15.3565	0.0004	0.0002	0.003	0.004	0.001	0.011	25.71	0.05	0.5	25.59	0.07	38.3	206.6	0.6
3.2	4.2439	0.0002	0.0007	0.012	0.018	0.002	0.011	25.51	0.20	0.2	25.46	0.29	10.6	205.6	2.2
3.5	6.0357	0.0005	0.0005	0.007	0.008	0.001	0.011	25.82	0.13	0.6	25.66	0.19	15.1	207.2	1.4
3.9	2.7927	0.0013	0.0011	0.037	0.023	0.004	0.011	25.76	0.19	1.4	25.39	0.38	7	205.1	2.9
4.2	1.5628	0.0010	0.0011	0.039	0.031	0.000	-0.011	25.92	0.27	1.1	25.64	0.42	3.9	207.0	3.2
4.6	0.9695	0.0014	0.0016	0.011	0.051	0.000	0.011	25.96	0.39	1.6	25.56	0.62	2.4	206.4	4.8
5.5	0.8875	0.0017	0.0031	0.033	0.051	-0.002	-0.011	25.92	0.43	1.9	25.43	1.02	2.2	205.4	7.8
15	1.5951	0.0015	0.0010	0.027	0.026	0.000	0.011	26.03	0.26	1.7	25.58	0.40	4	206.6	3.1
06AT111A01 Muscovite; J=.00426680 Gnawed Mountain Porphyry (Z9115)															
Aliquot B															
2.8	9.2947	0.0017	0.0004	0.155	0.015	0.004	0.011	27.93	0.27	1.8	27.43	0.29	9.2	199.6	2.0
3	7.997	0.0006	0.0003	0.000	0.002	0.005	0.011	28.36	0.32	0.7	28.17	0.33	7.9	204.7	2.3
3.5	20.1194	0.0004	0.0001	0.003	0.002	0.001	0.011	28.30	0.21	0.4	28.18	0.22	19.9	204.8	1.5
3.8	33.2721	0.0003	0.0001	0.000	0.001	0.004	0.011	28.24	0.13	0.3	28.15	0.14	33	204.6	0.9
4	3.8115	0.0014	0.0007	0.001	0.007	0.001	0.011	28.44	0.50	1.4	28.03	0.54	3.8	203.8	3.7
4.5	9.5443	0.0007	0.0003	0.001	0.001	0.003	0.011	28.22	0.56	0.8	28.00	0.56	9.5	203.6	3.9
5	3.9887	0.0004	0.0008	0.001	0.008	0.002	0.011	28.23	0.49	0.5	28.10	0.54	4	204.3	3.7
5.5	2.3034	0.0013	0.0015	0.002	0.009	0.009	0.012	28.45	0.68	1.3	28.07	0.81	2.3	204.1	5.6
15	10.572	0.0011	0.0003	0.025	0.009	0.003	0.011	28.43	0.26	1.2	28.10	0.27	10.5	204.3	1.9

Neutron flux gradients throughout the sample canister were evaluated by analyzing the sanidine flux monitors included with each sample packet and interpolating a linear fit against calculated J-factor and sample position. The error on individual J-factor values is conservatively estimated at ±0.6% (2□). Because the error associated with the J-factor is systematic and not related to individual analyses, correction for this uncertainty is not applied until calculation of dates from isotopic correlation diagrams (Roddick, 1988). No evidence for excess ^{40}Ar was observed in any of the samples and, therefore, all regressions are assumed to pass through the $^{40}Ar/^{36}Ar$ value for atmospheric air (295.5). If there is no evidence for excess ^{40}Ar the regressions are assumed to pass through the $^{40}Ar/^{36}Ar$ value for atmospheric air (295.5) and are plotted on gas release spectra. Blank were measured prior and after each aliquot and levels vary between ^{40}Ar=2.5-3.6x10^{-7} nm, ^{39}Ar=4.2-13.3x10^{-9} nm, ^{38}Ar=0.4-1.7x10^{-9} nm, ^{37}Ar=0.4-1.7x10^{-9} nm, ^{36}Ar=0.7-1.3x10^{-9} nm, all at ±20% uncertainty. Nucleogenic interference corrections are: $(^{40}Ar/^{39}Ar)_K$ =0.025±.005, $(^{38}Ar/^{39}Ar)_K$=0.011±0.010, $(^{40}Ar/^{37}Ar)_{Ca}$=0.002±0.002, $(^{39}Ar/^{37}Ar)_{Ca}$=0.00068±0.00004, $(^{38}Ar/^{37}Ar)_{Ca}$=0.00003±0.00003, $(^{36}Ar/^{37}Ar)_{Ca}$=0.00028±0.00016. All errors are quoted at the 2σ level of uncertainty.

Hornblende, biotite and/or muscovite were analysed from each of the main plutonic samples dated by the U-Pb method, results of which are presented in Table 3.

Highland Valley Suite

Guichon phase (sample 06WX010A02): Hornblende from this Guichon phase sample yielded a plateau age of 210.4 ± 2.6 Ma and an inverse isochron age of 208.5 ± 8.5 Ma, within error of the crystallization age (Fig. 8a, b). Biotite yielded a seven-step plateau age of 212.6 ± 2.6 Ma (Fig. 8c) within error of the 211.3 ± 0.7 Ma crystallization age determined for zircon (Fig. 6b). The similarity between the zircon, hornblende and biotite ages indicates rapid cooling of the intrusion and no post-crystallization thermal disturbance. The sample site is approximately 1.5 km northeast of the Bethlehem deposit.

Bethlehem Suite

Bethlehem phase (sample 06AT113A02): Hornblende from this Bethlehem phase sample yields a 213.7 ± 3.2 Ma plateau age and a reverse isochron age of 208.0 ± 4.2 Ma, within error of the zircon crystallization age at 210.3 ± 0.4 Ma (Fig. 8d, e). Analyses of two aliquots of biotite 06AT113A02 yield disturbed and uninterpretable spectrum (Fig. 8f). The disturbed spectrum and variable Ca/K ratios suggest alteration.

Bethsaida phase; (sample 06WX04A01): Analyses of two aliquots of biotite from this Bethsaida phase sample yielded reproducible plateaus with a combined plateau age of 210.1 ± 1.5 Ma (Fig. 8i). The age is within error of the crystallization age of 209.1 ± 0.3 Ma and indicates rapid cooling following crystallization with no obvious disturbance related to alteration and mineralization. Hornblende from this sample yields a plateau age of 223 Ma that is clearly older than the intrusion age (Fig. 8g). The plateau age is interpreted to be affected by excess argon as indicated by the non-atmospheric intercept on the inverse isochron (Fig. 8h). Inverse isochron regression yields an age of 208.2 ± 7.7 Ma Ma, similar to the biotite and within error of the zircon U-Pb age. The similarity of the three ages indicates rapid cooling from magmatic temperatures.

Gnawed Mountain subphase (sample 06AT111A01): Two analyses of muscovite from the Gnawed Mountain subphase sample yielded well defined plateau ages of 204.6 ± 1.3 Ma and 206.5 ± 2 Ma (Fig. 8j). This age is younger than the crystallization age of 208.6 ± 0.6 Ma determined for the dyke but similar to Ar ages for the sericite alteration assemblage within the Valley pit reported by Ash et al. (2007).

Geochemistry

Geochemical analyses were carried out at Geoscience Laboratories (Geolabs), Sudbury. Major elements were analyzed by fused disc XRF and FeO by titration. Trace elements were analyzed by Geolabs ICPMS packages IM100 and IM101. Information on precision and accuracy are available online at http://www.mndmf.gov.on.ca/mines/ogs/labs/default_e.asp.

A total of fifty-three samples from GCB were collected and analyzed for major and trace elements. The complete geochemical dataset, along with locations and additional descriptive information is available in Appendix 1. The seventeen representative analyses presented in Table 4 were mostly collected distal from mineralization and include the unaltered samples which were employed for geochemical modelling.

Table 4. Representative Analyses from the Guichon Creek Batholith.

Sample No.	WX05A1	WX20A2	WX41A1	WX45A1	AT115A1	AT114A1	WX10A1	WX13A1	WX16B1	AT113A1	WX24A1	WX04A2	WX03A1	WX40A1	WX07A1	WX26A1	AT111A3
Map Unit	<----------Border phase---------->				<----------Guichon phase---------->			Chataway	Bethleham phase		post-ore dyke	Bethsaida - Skeena subphase			Bethsaida	Gnawed Mtn porphyry	
Rock Type	gabbro	gabbro	qtz di	qtz di	qtz mzodi	gd	qtz mzodi	qtz mzodi	qtz di	gd	calcic tn	gd	gd	gd	gd	tn	calcic tn
Purpose[1]	HS-1		HS-2		HS-3	HS-5	U-Pb	HS-4	BS-i	U-Pb	BS-iii/U-Pb	U-Pb	BS-ii	BS-v	BS-iv	BS-vi	U-Pb
Major elements (wt.%)																	
SiO_2	50.9	51.5	58.4	60.1	60.4	66.6	61.3	65.1	64.6	65.9	71.0	68.0	69.1	72.3	70.8	70.7	73.5
TiO_2	1.19	0.87	0.70	0.82	0.71	0.49	0.67	0.53	0.44	0.34	0.30	0.27	0.29	0.18	0.22	0.17	0.14
Al_2O_3	19.19	19.45	17.84	16.22	16.55	14.45	16.68	15.77	17.37	16.49	16.46	16.04	16.22	15.09	15.83	15.77	14.98
Fe_2O_3	8.42	3.91	3.37	3.27	3.83	1.95	2.55	2.47	1.86	1.97	0.21	1.80	1.31	0.90	0.00	0.47	0.00
FeO	1.19	4.73	2.83	3.46	1.66	1.67	2.49	1.82	1.87	1.13	0.41	0.61	1.22	0.66	1.86	0.55	0.29
MnO	0.16	0.16	0.11	0.11	0.09	0.06	0.08	0.08	0.06	0.04	0.01	0.08	0.07	0.05	0.06	0.02	0.02
MgO	5.26	4.71	3.63	3.24	2.29	1.65	2.79	2.40	1.68	1.15	1.00	0.75	0.89	0.49	0.57	0.42	0.23
CaO	9.49	9.38	7.32	6.17	5.65	3.75	5.64	4.80	5.37	4.22	4.89	3.45	3.82	2.69	3.20	3.14	2.95
Na_2O	3.96	4.04	4.42	3.74	4.42	4.07	4.22	4.15	4.46	4.86	5.78	5.14	5.04	4.55	4.94	5.94	5.48
K_2O	0.20	0.49	1.32	1.86	2.24	2.95	1.96	2.46	1.86	1.94	0.24	1.85	1.90	2.92	2.19	0.98	0.44
P_2O_5	0.33	0.25	0.23	0.24	0.25	0.13	0.16	0.12	0.15	0.13	0.11	0.11	0.11	0.07	0.09	0.06	0.05
LOI	0.96	0.94	0.61	0.74	1.57	1.04	1.46	0.68	0.87	1.19	0.61	0.81	0.62	0.62	1.05	0.94	2.01
Total	101.21	100.42	100.79	99.98	99.67	98.76	100.02	100.39	100.60	99.40	101.05	98.87	100.62	100.50	100.85	99.20	100.11
Trace elements (ppm)																	
Cr	0	27	0	39	10	13	27	13	11	18	0	0	0	0	27	0	0
Ni	3	29	20	23	10	10	20	15	8	5	5	2	3	0	30	0	1
Co	5	26	18	18	13	9	15	12	9	6	2	4	5	3	28	2	0
Sc	4	16	12	15	10	7	12	10	7	5	4	3	4	3	21	3	2
V	49	217	147	169	119	90	127	105	72	61	52	42	49	28	241	25	19
Cu	7	74	30	274	49	171	100	184	156	292	11	4	5	45	147	160	676
Pb	5	6	4	5	7	8	5	4	4	4	2	5	4	7	2	4	4
Zn	33	72	62	68	55	42	45	43	42	22	9	39	34	28	92	16	12
Sn	0.4	2.1	0.6	0.6	2.1	2.7	0.6	0.8	0.4	1.1	0.6	0.4	0.4	0.3	0.5	0.3	0.9
W	0.1	0.3	0.0	0.0	0.3	0.2	0.2	0.1	0.1	0.6	0.8	0.1	0.1	0.0	0.1	0.0	1.8
Mo	0.8	1.9	1.2	2.7	2.5	2.1	1.4	1.2	1.4	5.0	1.6	0.4	0.7	0.9	0.5	5.2	15.5
Sb	0.1	0.5	0.2	0.2	0.2	0.3	0.2	0.1	0.1	0.2	0.3	0.1	0.0	0.1	0.0	0.5	0.1
Rb	36.3	10.8	25.5	49.5	52.8	74.4	44.6	66.5	47.8	30.9	1.5	30.9	27.4	52.8	1.3	10.2	5.4
Cs	0.6	0.7	0.6	1.5	0.9	1.3	0.8	1.8	0.9	0.6	0.2	0.5	0.5	1.1	0.1	0.6	0.3
Ba	977	435	506	1078	670	822	659	805	658	834	248	818	903	956	290	750	373
Sr	601	928	771	624	712	454	627	501	647	696	706	592	586	409	971	646	634
Tl	0.14	0.05	0.10	0.16	0.18	0.26	0.14	0.26	0.16	0.12	0.01	0.13	0.12	0.22	0.01	0.05	0.04
Ga	16.7	19.9	18.4	16.7	17.8	15.8	16.9	16.2	17.1	16.5	16.0	16.9	16.25	14.58	20.60	15.12	14.6
Li	6.3	7.1	7.0	12.4	8.2	12.9	7.1	9.1	10.9	5.8	1.7	11.9	5.0	9.6	4.9	7.5	7.9
Ta	0.0	0.0	0.0	0.2	0.2	0.2	0.0	0.2	0.0	0.0	0.2	0.0	0.0	0.2	0.0	0.0	0.0
Nb	2.2	1.0	2.0	2.9	4.4	3.1	2.4	2.7	1.8	1.9	2.3	2.2	2.1	2.2	1.5	1.6	1.8
Hf	1.5	0.8	1.6	5.4	2.0	3.5	1.3	2.0	3.0	2.0	2.1	1.4	1.1	1.8	0.6	1.4	1.4
Zr	36.4	26.5	47.0	219.0	67.0	124.4	36.8	57.1	113.2	64.9	73.0	36.8	27.7	50.0	15.2	45.0	45.2
Y	6.0	9.2	10.6	16.5	16.1	11.1	11.6	11.3	9.6	6.5	5.9	6.6	5.6	6.5	11.7	5.0	3.4
Th	2.2	0.7	2.6	3.2	3.5	6.4	2.9	5.9	3.0	1.9	2.4	2.0	1.3	2.9	0.1	0.7	0.6
U	1.2	0.4	1.1	1.5	1.7	2.7	1.4	3.3	1.4	1.3	1.5	1.0	0.7	1.0	0.1	0.5	1.1
La	8.74	7.98	11.17	14.21	19.25	15.57	12.21	12.24	9.12	8.97	3.71	10.04	8.46	10.94	8.76	5.78	18.89
Ce	17.99	17.30	24.80	33.00	43.51	33.79	27.88	27.98	20.39	19.35	9.70	20.69	18.13	21.20	20.46	11.80	25.89
Pr	2.18	2.27	3.31	4.39	5.42	4.15	3.56	3.62	2.63	2.39	1.45	2.48	2.15	2.36	2.93	1.43	2.12
Nd	8.88	10.51	14.63	19.88	21.77	16.74	15.02	14.92	11.24	9.83	6.36	9.52	8.44	8.85	13.95	5.59	6.29
Sm	1.74	2.35	2.98	4.12	4.33	3.30	3.08	3.06	2.37	1.91	1.33	1.71	1.61	1.53	3.17	1.07	0.81
Eu	0.50	1.04	0.95	1.16	1.14	0.76	0.86	0.73	0.66	0.57	0.45	0.49	0.49	0.49	1.19	0.44	0.30
Gd	1.33	2.20	2.46	3.49	3.56	2.63	2.58	2.51	2.09	1.47	1.10	1.31	1.28	1.22	2.88	0.91	0.62
Tb	0.20	0.31	0.35	0.50	0.52	0.36	0.38	0.37	0.30	0.21	0.16	0.19	0.18	0.17	0.42	0.14	0.09
Dy	1.11	1.84	1.90	2.70	3.11	2.13	2.24	2.17	1.82	1.22	1.00	1.12	1.05	1.00	2.43	0.80	0.55
Ho	0.21	0.36	0.38	0.55	0.60	0.42	0.44	0.43	0.36	0.24	0.19	0.22	0.21	0.20	0.47	0.16	0.12
Er	0.63	0.99	1.00	1.55	1.70	1.20	1.25	1.23	1.05	0.70	0.52	0.66	0.61	0.58	1.29	0.45	0.36
Tm	0.09	0.14	0.16	0.24	0.25	0.18	0.18	0.19	0.16	0.10	0.09	0.10	0.09	0.10	0.18	0.08	0.06
Yb	0.66	0.88	1.00	1.60	1.61	1.21	1.16	1.25	1.06	0.72	0.60	0.71	0.61	0.74	1.11	0.55	0.45
Lu	0.10	0.13	0.15	0.25	0.24	0.19	0.17	0.19	0.17	0.11	0.10	0.11	0.09	0.13	0.16	0.09	0.08
Be	1.09	0.60	0.80	0.79	1.03	1.10	0.85	1.04	0.79	0.86	0.97	1.19	1.00	0.86	0.74	0.97	0.81
K_2O/Na_2O	0.051	0.121	0.299	0.497	0.507	0.725	0.464	0.593	0.417	0.399	0.042	0.360	0.377	0.642	0.443	0.165	0.080
Sr/Y	100.9	101.0	72.7	37.9	44.2	40.9	53.8	44.3	67.6	107.3	120.1	89.8	104.7	63.2	83.0	129.7	187.6
La/Yb	13.2	9.1	11.2	8.9	12.0	12.9	10.5	9.8	8.6	12.5	6.2	14.1	13.9	14.8	7.9	10.5	42.0
WR Mg#	52	50	52	47	44	46	51	51	46	41	75	37	40	37	35	44	59

1. Representative analyses were either employ for geochemical modelling or U-Pb dating, or both. Compositions employed in Highland Valley and Bethleham modelling are labelled HS-1 to 5 and BS-I to vi, respectively (see Appenix 2 and Fig. 10). Note that 06 and 07 prefixes and extra zeros were dropped from sample numbers.
Rock types: di - diorite; gd - granodiorite; mzodi - monzodiorite; tn - tonalite; qtz - quartz. Lithologies based on Q'-ANOR classification scheme of Streckeisen and LeMaitre (1979) shown in Fig. 3.

Major and trace elements

The compositional diversity of plutonic units within the GCB is illustrated in a major element-based plutonic rock classification diagram (Fig. 3). Herein the two geochemical suites previously recognized by McMillan (1985) are termed the Highland Valley (HVS) and Bethlehem (BS) suites (see inferred trends in Figures 3 and 4). The two suites define separate but approximately parallel trends in the Q'-ANOR diagram with the HVS being calc-alkalic and the BS being more calcic. All but one non-dyke GCB sample is magnesian (Fig. 4a) and all but three altered Gnawed Mountain porphyry samples are metaluminous. In general, HVS phases have >60 wt.% silica and are more magnesian than either the BS or HVS Border phase at comparable SiO_2 compositions. In their alkali-lime indices, HVS samples straddle the calcic – calc-alkalic boundary whereas younger BS samples plot almost exclusively within the calcic field and become more calcic as silica content increases (Figs. 3 and 4b). With the exception of some dyke samples and mafic Border phase samples, both GCB suites are medium-K (Fig. 9).

The two suites display distinct and well defined linear trends in major and trace element Harker variation diagrams presented in Figures 9 and 10, The older HVS has higher K_2O, TiO_2, FeO^{total}, MgO, Mg#, K_2O/Na_2O, Sc, Rb, Th, Zr, La and Yb and lower Na_2O, Al_2O_3 and Sr contents than the BS at comparable SiO_2 contents (i.e., 65 to 70 wt.%). For many elements, HVS Border phase compositions plot on or near the lower-silica projection of the Guichon and Chattaway subphase trend, the exceptions being

Na_2O, Sr, Rb, Zr, Mg# and K_2O/Na_2O. These features are incompatible with the two suites having formed from compositionally similar parental magmas. This and the ~3 M.y. time gap between the Border and Guichon phases are incompatible with the Border phase and other HVS phases being co-genetic.

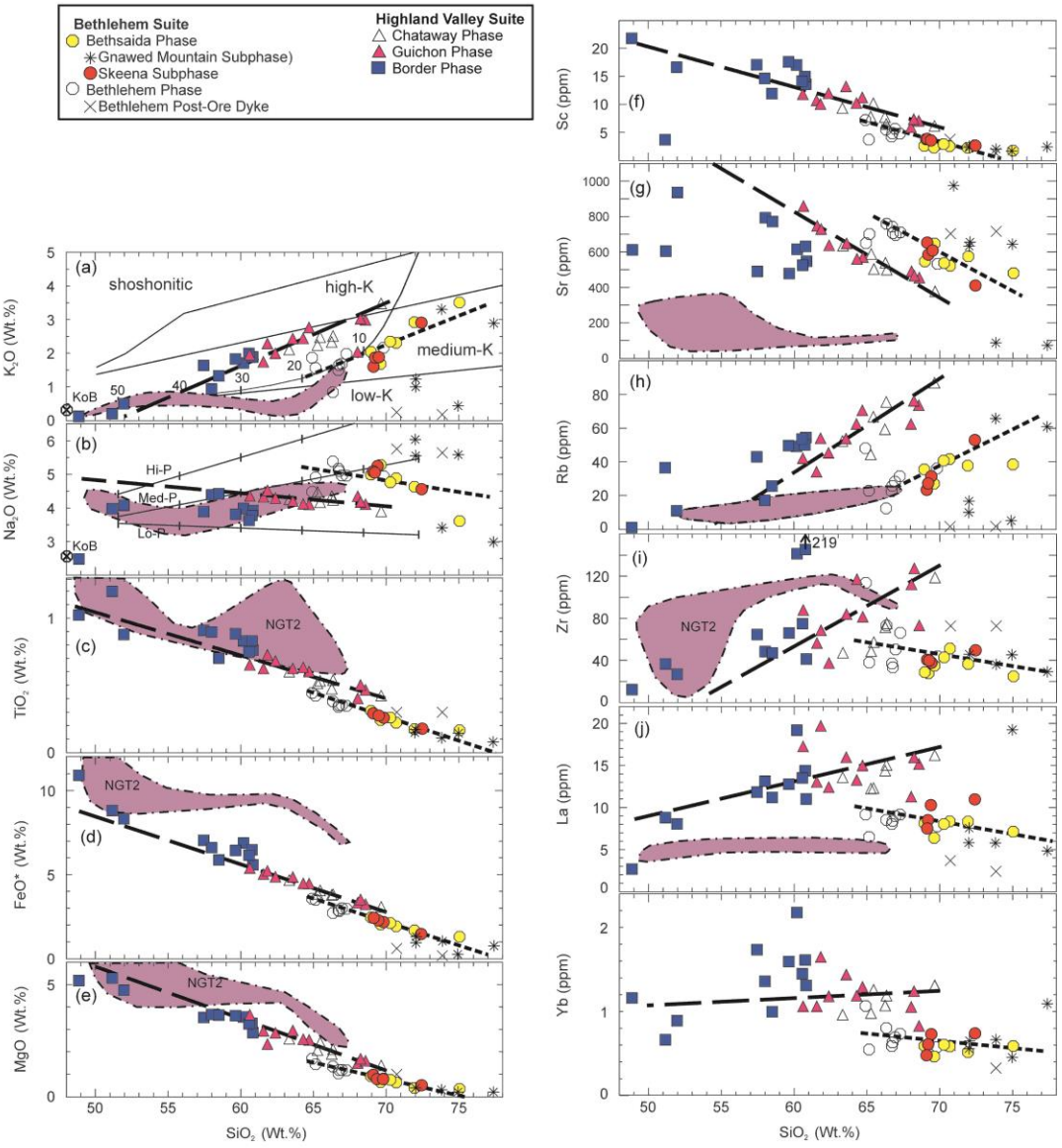

Figure 9. Selected Harker variation diagrams for the Guichon Creek Batholith. Symbols and inferred trends for HVS and BS as in Fig 3. Note that the projection of the HVS trend to lower silica levels may or may not conform to the distribution of mafic Border phase compositions. Also shown, outlined with a solid line, is the field for Nicola Group type 2 224-210 Ma low-K calc-alkaline lavas (NGT2; N=8) from Mortimer (1987).

Normalized-extended-element plots for GCB suites are shown in Figure 11. The most distinctive features are the enrichment of light rare earth (LREE) and large-ion lithophile elements (LILE) (e.g. Rb, Ba, K), with well-developed negative Nb and flat to slightly negative Zr and Ti anomalies. In general, the BS suite is less enriched in incompatible elements with lower overall REE abundances and distinctly lower HREE.

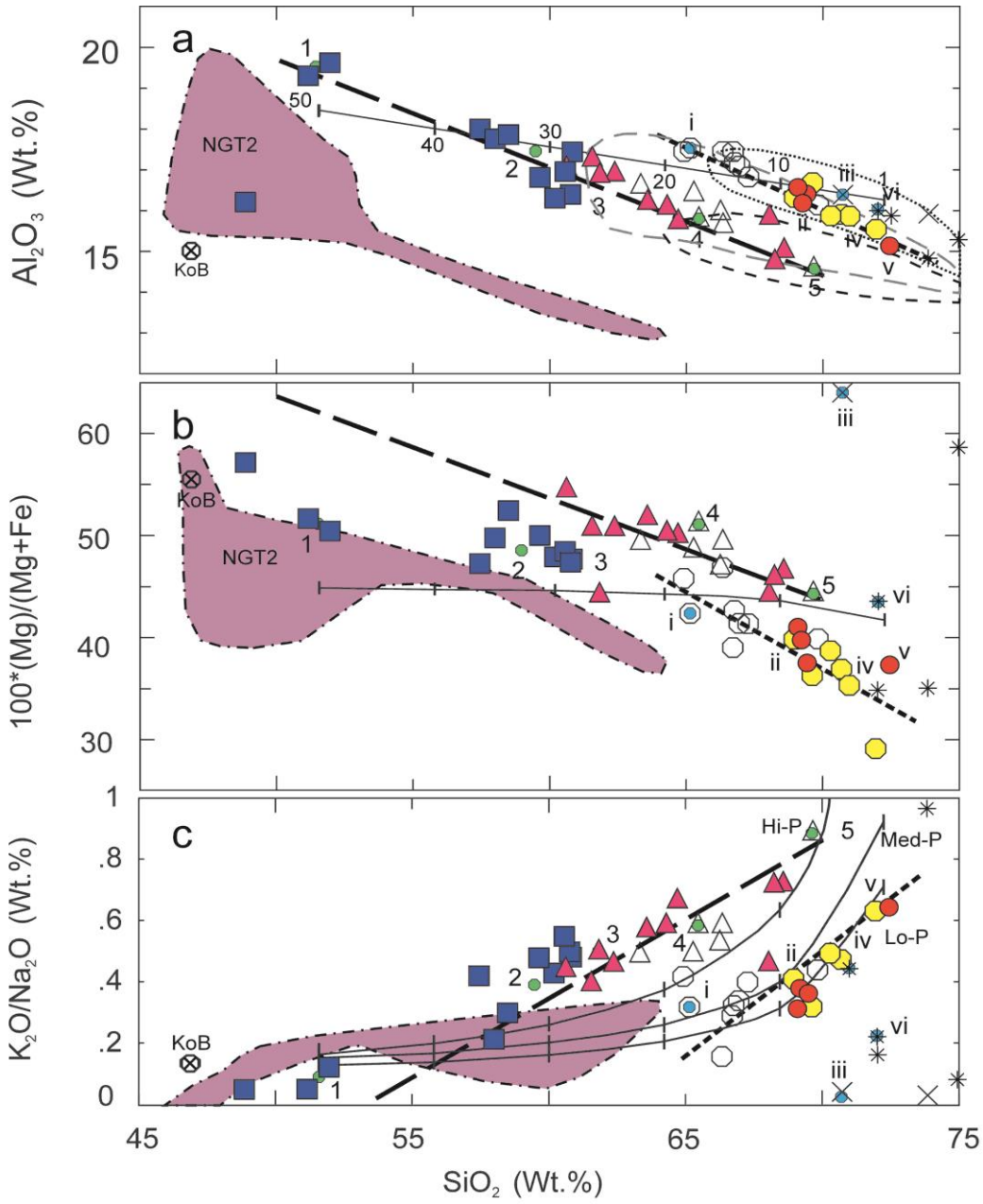

Figure 10. Harker variation diagrams for the Guichon Creek Batholith for; (a) Al_2O_3; (b) 100*(Mg/(Mg+Fe); and (c) K_2O/Na_2O. Symbols, fields and inferred trends as in Figs 3 and 9. Also indicated with green and blue dots are geochemical modelling samples. Highland Valley and Bethleham suite samples employed for geochemical modelling are labeled 1 to 5 and i to v, respectively, and shown in Table 2.

Almost all BS samples display very pronounced positive Ba and Sr anomalies whereas within the HVS these anomalies are much less well-developed. Normalized REE patterns are generally similar, with the BS having lower abundances and a more pronounced concave-up HREE pattern. Sr and LREE enrichment relative to HREE (and Y) is highlighted by elevated Sr/Y (HVS= 49 ± 13 and BS= 100 ± 21) (Fig. 12) and

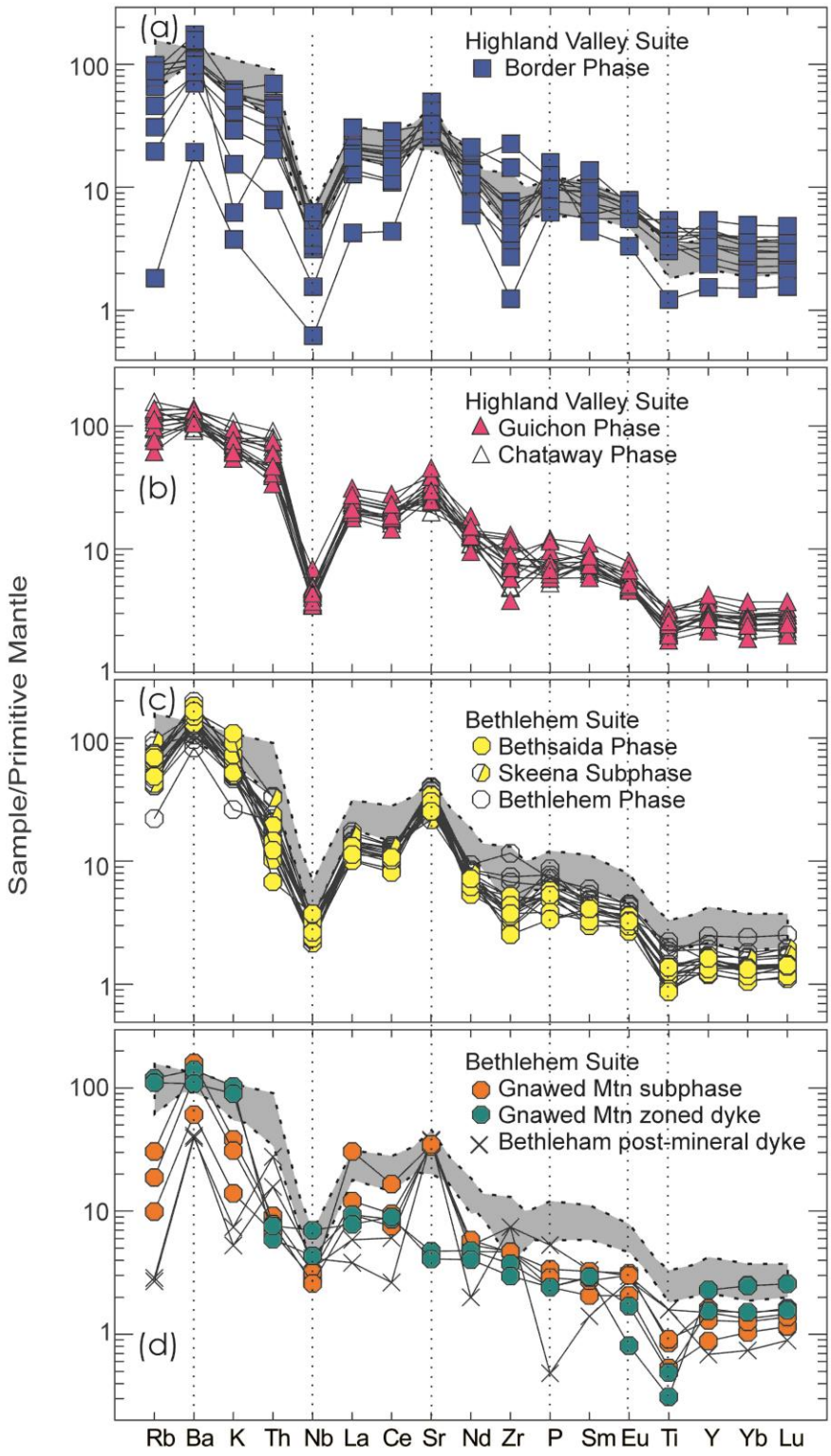

Figure 11. Primitive mantle normalized extended element plots for Guichon Creek Batholith plutonic units. For comparison purposes, the field from (b) for felsic Highland Valley suite phases is also shown in (a), (c) and (d). Primitive mantle normalizing values are from Sun and McDonough (1989).

moderate La/Yb ((HVS= 11.0 ± 3.0 and BS= 13.0 ± 6.5) signatures (Fig. 11; see Table 2). Sr content, and to a lesser extent Sr/Y, decreases with increasing SiO_2 so that the least evolved phases of each suite have the highest Sr/Y and Sr contents. BS high Sr/Y and low HREE features are considered to be characteristic of 'adakites' (Defant and Drummond, 1990). Based on Sr/Y ratios, HVS rocks have compositions that plot at the lower end of the adakite field, with some Border phase samples falling within the higher end of the typical arc field, whereas BS rocks have higher Sr/Y and lower HREE and plot well within the field of adakites (Fig. 12).

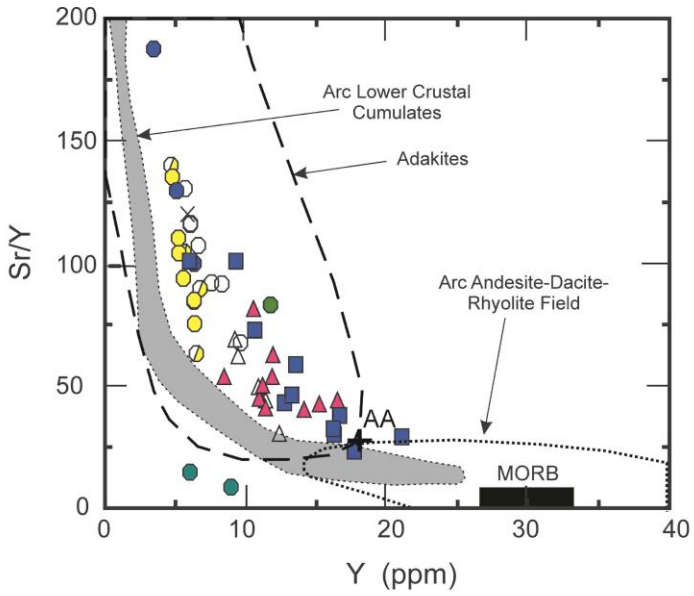

Figure 12. Sr/Y-Y plot for the Guichon Creek Batholith. Fields for adakites and arc andesite-dacite-rhyolite from Richardson and Kerrich (2007), as is the average medium-K arc andesite (AA). The field for arc lower crustal cumulates is based on the data of Greene et al. (2006). Plutonic unit symbols as in other plots.

Nd and Sr isotopes

Nd tracer isotopic analyses reported in Table 5 were conducted using the multicollector ICP-MS Nu Plasma™ at the Geological Survey of Canada. Samarium and neodymium were analyzed using an array of fixed Faraday collectors in static multicollector mode. The isotopic ratios were corrected for spike contribution and mass discrimination by numeric solution of the isotope dilution equations with exponential normalization. Quality control was performed by monitoring the uniformity of non-radiogenic isotopic ratios and by analyzing of standards (La Jolla Nd and Ames Sm).

A subset of ten of the geochemical samples from Highland Valley and Bethlehem suites were selected for Nd isotopic analyses (Table 3). Epsilon Nd values have been calculated at the time of emplacement ($\varepsilon_{Nd}(T)$) based either on measured U-Pb zircon ages or approximate ages. Depleted mantle model ages (T_{DM}) were calculated following the model of DePaolo (1981). In general, ε_{Nd} (T) values range from +6.3 to +8.1 and T_{DM} ages span from 195 to 534 Ma. With the exception of the Nd isotopic composition of the strongly positive ~ 3 M.y. older Border phase sample (06WX014A01), all values (+6.3

to +7.3) overlap within analytical error of ±1 epsilon unit, as indicated by duplicate analyses (+4.9 and +6.0) on sample 06WX015A01. Consistently positive ε_{Nd}(T) values indicate that both GCB suites were derived from a crustal reservoir with a short-term history of light REE enrichment. Published initial $^{87}Sr/^{86}Sr$ values for 10 Bethlehem suite whole rock samples range from 0.7032 to 0.7037 (Preto et al., 1979), supporting GCB derivation from juvenile/mantle-like sources. The most juvenile Border phase sample (ε_{Nd} = +7.3) indicates input from depleted-mantle-like mafic magma, but the lack of significant change in ε_{Nd} over a SiO_2 range of 51.5 to 73.5 wt.% argues against input from isotopically evolved (i.e., negative ε_{Nd} and high initial $^{87}Sr/^{86}Sr$) materials (e.g. ancient North American crust) during its petrogenesis.

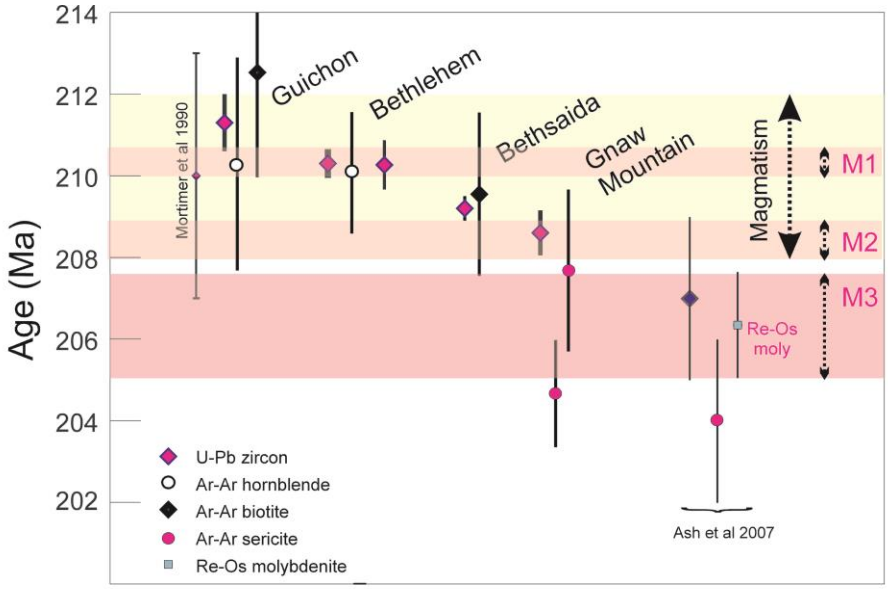

Figure 13. Summary of age results with three inferred periods of mineralization (M1, M2, M3). Data from this paper, Mortimer et al. (1990) and Ash et al. (2007).

Discussion

Age and Evolution of the Guichon Creek Batholith

The principal phases of the Guichon Creek Batholith (GCB) were emplaced and evolved over a 7 M.y period between 215 and 208 Ma. The duration of magmatism is typical of recent estimates of 2 to 10 M.y. for the construction of large plutonic complexes in continental margin settings (e.g., de Silva and Grosnold, 2007; Lipman, 2007). Well studied specific examples include the Tuolumne (10 M.y.; Coleman et al., 2004) and Mt. Whitney (8 M.y.; Hirt, 2007) normally compositionally zoned plutonic complexes of the Sierra Nevada batholith. The individual GCB intrusive phases underwent rapid cooling below the closure temperature for Ar in biotite, consistent with interpretations of relatively shallow intrusive levels suggested in the earlier work on regional structural setting (e.g., Northcote, 1969; McMillan, 1976). The hydrothermal systems are highly focussed and do not appear to significantly affect the argon systematics in samples adjacent to mineralized zones.

Zircon preserves a relatively simple magmatic history with little evidence for major resorbtion or inheritance of significantly older basement rocks. Inheritance is limited to ages of ~216-220 Ma that may represent slightly older magmatic phases within the Triassic arc such as the roots to the Carnian-Norian Nicola Group volcanic arc. This is in accord with the Nd and Sr isotopic evidence that does not indicate involvement of pre-Paleozoic crust in the development of these magmatic rocks.

Timing of Alteration and Mineralization

MacMillan (1985) interpreted several phases of mineralization within the Highland Valley deposits. Based on our new and existing geochronological data, at least three temporally distinct phases of mineralization can be associated with the intrusion and cooling of GCB (Fig. 13).

(1) Mineralization at the Bethlehem pit occurred over an 800 ka period at 210.3 Ma, defined by the age of the host intrusion at 210.3 ± 0.4 Ma and the age of a cross-cutting non-mineralized dyke at 210.3 ± 0.6 Ma. Mineralization at Bethlehem had, therefore, terminated prior to intrusion and crystallization of the Bethsaida phase of the batholith.

(2) Mineralization in the deposits hosted by the Bethsaisda phase (Highmont, Lornex, Valley, JA) occurred after 209.1 ± 0.3 Ma, the age of the Bethsaida sample. The 208.6 ± 0.6 Ma age for the Gnawed Mountain subphase, one of the youngest intrusive phases in the area, and interpreted to be late to syn-mineralization by McMillan (1985), suggests that mineralization at Highmont occurred at or slightly before ca. 208.6 ± 0.6 Ma. The estimate of the age difference between the Bethsaida and Gnawed Mountain subphase is 0.55 +0.6/-0.5 Ma, suggesting that mineralization occurred within a 1.1 Ma interval at approximately 209 Ma. This is supported by previously reported Ar-Ar hydrothermal biotite ages from the Valley pit that record a 207 ± 2 Ma age, within error or slightly younger than the age of the Gnawed Mountain suphase. The slightly younger biotite age may reflect slower cooling of the hydrothermal system, systematic differences attributable to analytical calibration (e.g., Jourdan and Renne, 2007), or possibly partial resetting during molybdenite mineralization at 206 Ma (see below)

(3) Molybdenite from the Valley Pit has a Re-Os age of 206.3 ± 1.2 Ma (Ash et al. 2007; recalculated as the weighted average of replicate molybdenite ages reported by Ash et al. 2007; decay constant error included). The molybdenite is from a massive, 8 to 10 cm wide, steeply dipping vein on the southeastern corner of the Valley Pit. This style of molybdenum mineralization is interpreted to be relatively late in the mineral paragenesis (McMillan, 1985) and thus its Re-Os date provides a minimum age on the earlier disseminated Cu mineralization at the Valley Pit. The molybdenite age is significantly younger than the youngest intrusive rock dated in the area, the late-syn mineralization Gnawed Mountain subphase at 208.6 ± 0.6 Ma. If this interpretation is correct, then mineralization at Highmont is at least 2.4 ± 1.3 M.y. older than molybdenite vein mineralization in the Valley Pit.

Although not specifically targeted to mineralization, the sericite Ar-Ar data from the Highmont deposit (Table 3) and that of Ash et al. (2007) from the Valley Pit support the above interpretation. The Ar-Ar ages for hornblende and biotite give similar ages to the U-Pb zircon crystallization ages suggesting that

the regional thermal gradient was tightly focused on the fault-controlled zones of mineralization and that the plutons cooled rapidly to below biotite closure temperatures within measure of the analytical precision. In summary, the geochronological data suggest that mineralization within Highland Valley District developed intermittently between 210 and 206 Ma via at least three temporally discrete mineralizing events at: (a) 210.3 ± 0.8 Ma (Bethlehem); (b) between 209.1 and 208.6 Ma (Highmont, Lornex, Valley), and; (c) vein molybdenite mineralization in the Valley pit at 206 ± 1.2 Ma (Ash et al., 2007). The duration of each of these GCB events was relatively short, with best estimates being less than 1 M.y. Based on Lee et al. (2017) and references therein, porphyry ore-related magmatism ranges from short-lived (1M.y. or less) single episodes, to long-lived (up to 8 M.y.) multiple igneous-related mineralizing events. This is in accord with estimates of the duration of hydrothermal systems from theoretical considerations (100-500 ka; e.g. Cathles and Shannon, 2007).

Petrogenesis and Evolution of Parental Magmas

Geochemical Modelling Techniques

Geochemical modelling was carried out employing carefully selected unaltered samples that were collected distal from mineralization and which exhibit low loss on ignition (LOI) levels that correlate based on their silica content, ranging from SiO_2 = 60 wt.% with LOI = 1.6, to SiO_2 = 72 wt.% with LOI = 0.62. This needs to be keep in mind when evaluating the trace element modelling which does include some relatively mobile elements such as Rb, Sr and Ba. To facilitate major element modelling electron microprobe major element analyses of minerals (feldspar (108), pyroxenes (43), amphibole (103), biotite (78) and magnetite (38)) were obtained from 11 samples at the Geological Survey of Canada. Four of the microprobed samples were employed in the modelling. As no consistent compositional zoning was identified within individual mafic silicate grains, grain or domain analyses were averaged for comparison between samples and for modelling (see Appendix 2). Modelling was carried out for both major and trace elements employing sample compositions presented in Table 4 and plotted in Figure 10. They are numbered 1 to 5 for the HVS and i to vi for the BS, by which they are referred to below.

(i) Partial Melting Modelling

GCB partial melting modelling was based on an experimental study of Archean TTG (tonalite-trondhjemite-granodiorite) petrogenesis by Moyen and Stevens (2006), as TTG compositions share many compositional similarities with higher silica GCB plutonic units. For the Bethlehem suite (BS), major element modelling found a quite close correspondence between a 20% partial melt of the komatiitic basalt (KoB) protolith of Moyen and Stevens (2006) (their Table 3) and low silica BS composition (i) (Figs. 9a,b and Fig. 10) (Appendix 3). As Na_2O and K_2O/Na_2O of melts are pressure (P) dependent, modelling suggests that melting to produce the BS likely occurred under medium to high pressure (garnet-amphibolite) conditions. For the Highland Valley suite (HVS), which is characterized by higher K_2O, K_2O/Na_2O and lower Na_2O than the BS, generation of the lower silica Guichon phase composition (3) by 20 to 25% partial melt of the tholeiitic basalt (THB) protolith of Moyen and Stevens (2006), under low- to

medium pressure conditions, provided a reasonable fit. Equilibrium partial melting modelling of trace elements required some modification of the source trace element compositions of Moyen and Stevens (2006) (their Table 3). Preferred results of the trace element partial melting modelling are given in Appendix 3. In summary, good fits were obtained for: (1) a 20% partial melt of komateiitic mafic composition (KoB) to produce BS composition (i) with a restite of 50% amphibole and 20% garnet; and (2) a 20% partial melt of a tholeiitic mafic composition (ThB) to produce HVS composition (3) with a restite of 60% amphibole and 10% garnet.

(ii) Crystal Fractionation Modelling

Employing program XLFRAC (Stormer and Nicholls, 1978) for least squares major element modelling, a spectrum of initial and final magmas from GCB whole rock analyses were tested (see Fig. 10 and Table 4). The cumulate mineralogy and mineral compositions from probe analyses were varied so as to improve model fit, as indicated by a low sum of the squares of the residuals (SSR). The best fit major element fractional crystallization models were subsequently tested employing Rayleigh fractionation for a range of compatible and incompatible trace elements (Appendix 4).

Modelling indicated that the Border phase of the HVS consists of cumulate-melt mixtures not liquid compositions and cannot be employed to generate more felsic HVS compositions by fractional crystallization. For more felsic HVS phases, excellent fits of least squares of residual (LSSR) of between 0.20 and .002 were obtained for models that produced higher silica Chataway and Guichon phase compositions (4) and (5) from mafic Guichon composition (3). For HVS models involving <65 wt.% SiO_2 compositions, plagioclase, two pyroxenes and magnetite were the main minerals, with hornblende being either absent or <3% of 80-90% subtracted solids. Amphibole became a significant fractionated phase, in abundance ratio of 2:1 with clinopyroxene, only when end-member compositions contained >65 wt.% SiO_2. Biotite, quartz and K-feldspar were not required as subtracted phases. In BS major element modelling, initial Bethlehem phase composition (i) was employed to derive via fractionation more evolved BS compositions (ii) to (vi) for which good quality fits of SSR between 0.42 and 0.002 were obtained. Modelling of mafic to intermediate BS compositions involved removal of mainly plagioclase and amphibole and minor clinopyroxene and magnetite. Evolution to >70 wt.% silica BS compositions required the addition of quartz, K-feldspar and biotite to the solids.

Rayleigh trace element fractionation modelling employed weight percents of mineral solids and fractionation (F) values obtained in the major element modelling. Modelling in which mafic Guichon phase composition (3) was employed to derive more felsic HVS compositions (3) and (5) yielded reasonably good degrees of fit for trace elements such as Sr, Ba and Rb that are controlled by major rock forming minerals. With the addition of accessory minerals such as zircon, reasonable degrees of fit were obtained for other trace elements such as Y, Zr, Nb, Th, U and REE. In BS modelling employing lower silica BS composition (i) to derive higher silica compositions (ii) to (vi), trace element fits were not as good as those for the HVS. This may reflect the higher silica and more water-rich magma compositions involved for which partition coefficients can be variable and accessory phases play a greater role.

Modelling summary and implications

Partial melting was employed to evaluate a lower crustal petrogenesis for Guichon Creek Batholith Highland Valley (HVS) and Bethlehem (BS) primary magmas (see Appendices 3 and 4). In general, this modelling indicated: (a) the more elevated Al_2O_3, Na_2O, and Sr concentrations and Sr/Y values (Table 4; Figs. 10 to 12) exhibited by the BS than the HVS could reflect the BS being produced from mafic sources under medium to high P-T conditions versus low to medium P-T conditions for the HVS; (b) initial magmas for HVS and BS could have been generated by lower crustal partial melting of komatiitic and tholeiitic basaltic protoliths characterized by La/Yb values of 0.67 and 1.55, respectively; and (c) residual mineralogies of 60% amphibole and 20% garnet for the BS and 70% amphibole and 10% garnet for the HVS, with both suites lacking residual plagioclase. For certain late Gnawed Mountain porphyry samples, distinctively higher La/Yb ratios and low Yb (Table 4) require an eclogitic residue, if they were derived from protoliths similar to other BS phases.

Unsuccessful fractionation modelling of the Border phase indicated that it consists of cumulate-melt mixtures, not liquid compositions, which, due to its ca 215.6 Ma emplacement age, cannot be interpreted as being generated from evolution of younger (ca 211.3 Ma) HVS phases. However, major element modelling of the younger felsic HVS and BS phases indicated that their compositional variation can be modeled by low-pressure crystal fractionation. In the case of the HVS Guichon and Chataway phases, it indicates that felsic compositions can be derived from an intermediate composition magma (~59% SiO_2) by a two-stage process characterized by initial fractionation of plagioclase, two pyroxenes and magnetite, with <3% hornblende; followed by fractionation of plagioclase and amphibole with lesser clinopyroxene (see online Appendices 5 and 8). Major element modelling of the BS starting with a magma composition at ~65% SiO_2 requires removal of mainly plagioclase and amphibole with minor clinopyroxene and magnetite. Modelling of sample compositions with >70 wt.% silica requires the addition of quartz, K-feldspar and biotite to the solids.

Within suite trace element modelling based on the major element models yields acceptable degrees of fit for trace elements such as Sr, Ba and Rb that are controlled by major rock forming minerals; whereas the addition of accessory minerals such as zircon, is required to account for other trace elements such as Y, Zr, Nb, Th, U and REE. In general trace element models for BS compositions have poorer overall fits than those for the HVS. This may reflect the higher silica and more water-rich magma compositions involved for which partition coefficients can be variable and accessory phases play a greater role. The major element and trace element modelling suggests that HVS evolution occurred via shallow level fractional crystallization of anhydrous minerals with amphibole on the liquidus at relatively late stages of crystallization. In contrast, modelling of the BS indicates that amphibole fractionation occurred during all stages of BS formation. Thus, the BS parental magmas were initially water-rich to water-saturated.

In summary, mineralization within the Guichon Creek Batholith coincides in time with previously described changes in magma composition from the Highland Valley suite (HVS) to the Bethlehem suite (BS). Geochemical modelling (see Appendices 3 and 4) indicates that the two magmatic suites cannot be

fractionation products from a common parental magma, but rather represent distinct magma batches with independent partial melting, mingling and fractionation processes.

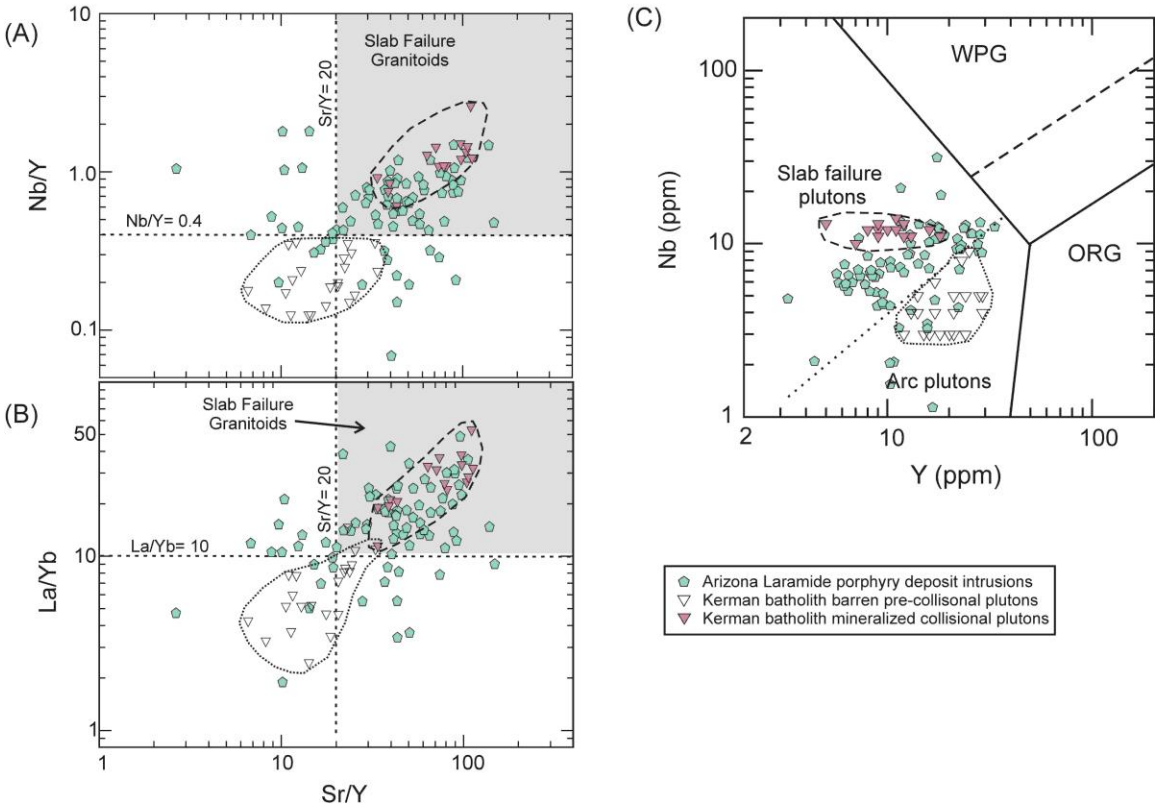

Figure 14. Sr/Y vs (a) Nb/Y and (b) La/Yb and (c) Y vs Nb discrimination plots of Hildebrand and Whalen (2014) for Arizona Laramide porphyry Cu intrusions (data of Lang and Titley, 1998) and barren arc-related pre-collision plutons and post-collision porphyry Cu-related intrusions of the Cenozoic Kerman batholith, Iran (data of Shafiei et al., 2009).

Tectonomagmatic Characterization of Fertile Plutonic Suites

The classification and petrogenesis of high Sr/Y magmas in arc settings remains a subject of considerable debate (Martin et al., 2005; Richards and Kerrich, 2007; MacPherson et al., 2006). Rocks with these compositions have been attributed to slab melting and wedge interaction during the subduction of young, hot oceanic crust (Drummond and Defant, 1990; Martin et al., 2005). However, magmas with high Sr/Y and low Y compositions can equally well be produced by a variety of deep crustal processes involving medium to high pressure partial melting or fractionation of mafic amphibolites (± residual garnet; see Moyen, 2009). A potential association of low Y, high Sr/Y felsic arc magmas with major Miocene porphyry Cu deposits was recognized decades ago (e.g., Baldwin and Pearce, 1982). Since then, this linkage has been well substantiated by additional studies, including that of Bissig et al. (2017). In their study, an oxidized, high Sr/Y, restitic garnet-bearing, granodiorite suite, strongly evidenced as a product of

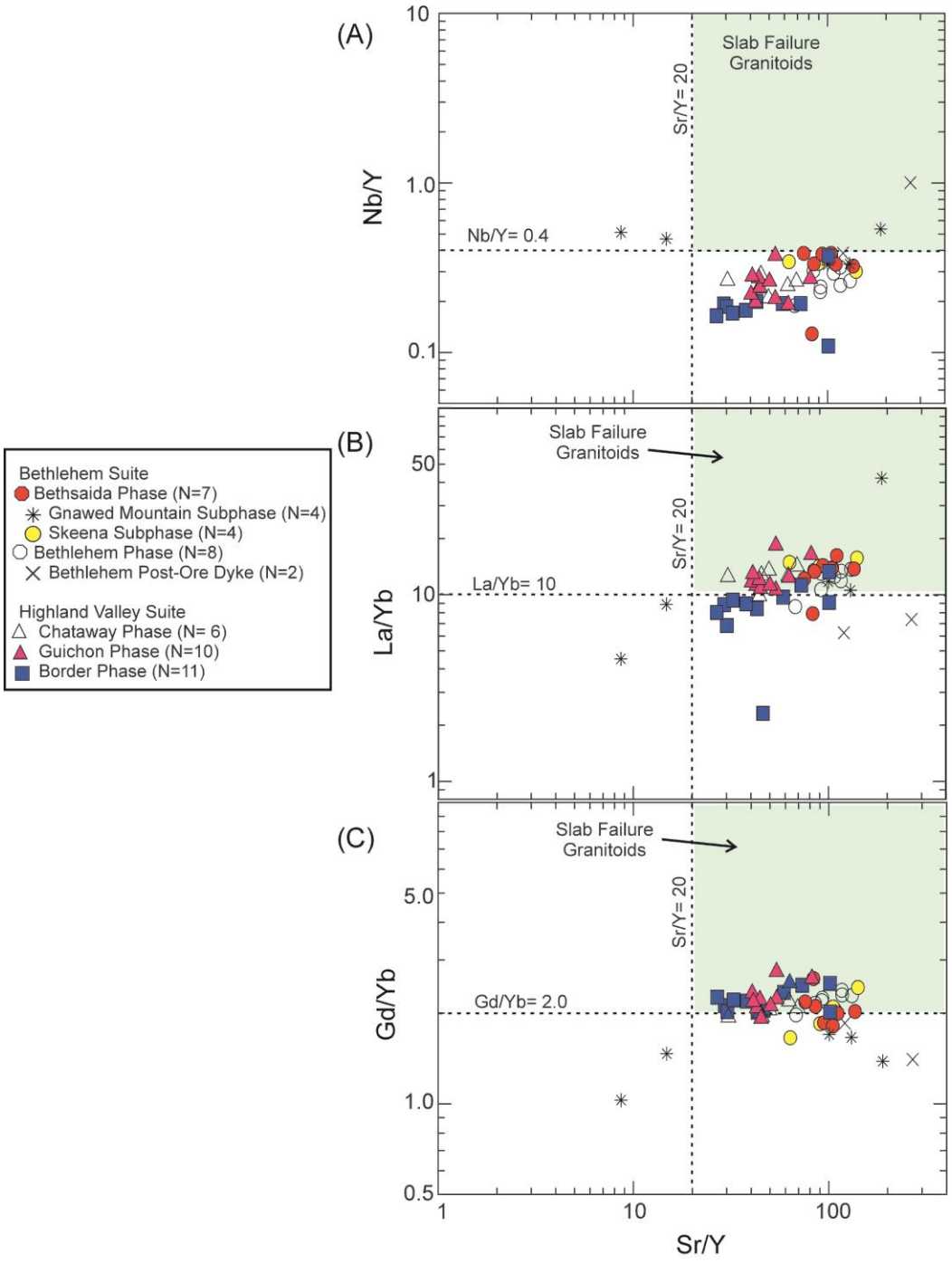

Figure 15. Sr/Y vs (a) Nb/Y, (b) La/Yb and (c) Gd/Yb discrimination plots of Hildebrand and Whalen (2014) for Guichon Creek batholith plutonic phases.

high P (>1 GPa) lower crustal petrogenesis, was shown to be the progenitor to Au-Cu porphyry mineralization. Some authors have drawn a causal link between fertile high Sr/Y intrusions and slab-melting processes (e.g., Sajona et al., 2000). However, Richards and Kerrich (2007) argued that few high Sr/Y intrusions associated with porphyry systems could be demonstrated to be derived by slab melting and

suggested that such magmas represent products of thickening and melting within the sub arc lithosphere as the natural consequence of arc maturation. Alternative models for these magmas include being due to collisional thickening, ridge subduction (Hollings et al. 2005) and resulting from changes in slab dip and subduction erosion (Kay et al. 2005). More recently, Hildebrand and Whalen (2014; 2017) have interpreted these 'adakitic-like' post-collisional granitoid magmas as products of slab failure (SF) and identified distinctive geochemical signatures, including elevated Sr/Y, La/Yb, Gd/Yb and Nb/Y, for distinguishing them from pre-collisional arc magmatism. As well, Hildebrand (2013) recognized that SF magmatism can be progenitors to economically important mineralization, including Arizona Laramide porphyry Cu-Mo and Cu-Au deposits (Fig. 14). An excellent example of a change from barren arc-related plutonism to fertile porphyry deposit hosting SF magmatism is the Eocene-Oligocene Kerman batholith of central Iran. Pre-collisional unmineralized diorite to granodiorite intrusions and volcanic equivalents are followed by collisional adakite-like porphyritic granodiorites that host some of the world's largest Cu ore deposits (Shafiei et al., 2009). These magmatic pulses plot as separate arc and slab failure groups on discrimination diagrams of Hildebrand and Whalen (2014, 2017) (Fig. 14), supporting their interpretation of the origin and economic significance of high Sr/Y SF plutonic suites.

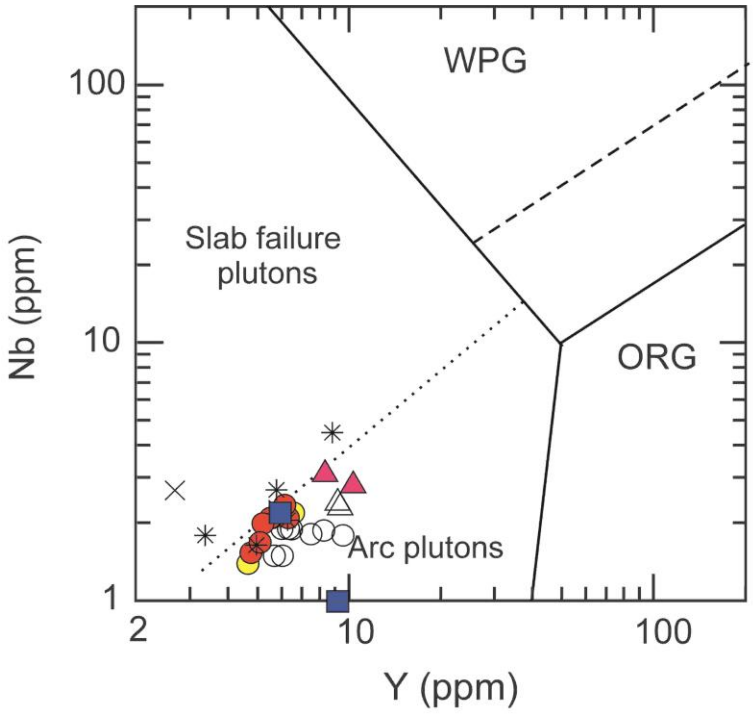

Figure 16. Y vs Nb discrimination plot for Guichon Creek Batholith plutonic phases. Plots after Hildebrand and Whalen (2014), but modified from Pearce et al. (1984). Plutonic unit symbols as in Fig. 15.

In a summary of slab failure processes, Hildebrand and Whalen (2014) highlighted that once the subducting slab detaches; (a) asthenosphere upwells through the tear, melts adiabatically and rises into the collision zone; (b) high temperature asthenospheric mafic magmas initiate large scale partial melting of subcontinental mantle lithosphere and deep crust of the overlapping lower and upper plates; (c) resultant SF

magmas are emplaced mainly into the upper plate as a linear array above the trace of the tear in the descending slab; (d) rocks of the partially subducted lower plate rapidly rebound due to buoyancy forces; and (e) SF magmatism commonly overlaps terminal stages of collisional deformation, or post-dates collision-related structures.

GCB features that can be interpreted as compatible with this SF magmatism model are:

(a) Significant uplift and erosion of GCB shortly after emplacement, is evidenced by a regional unconformity between the subaqueous lower and subaerial middle to upper Nicola Group and the Lower to Middle Jurassic Ashcroft Formation that unconformably overlies the GCB (Fig. 2). These features can be explained by rebound of the upper plate, into which the GCB was emplaced, following detachment of the slab from the underthrust lower plate.

(b) In its normal compositional zoning from outer more mafic (gabbro/diorite) Border to interior more felsic Bethsaida (granodiorite/tonalite) phases, the Guichon Creek Batholith (GCB) resembles other Cordilleran slab-failure plutonic complexes such as the La Posta suite Sierra San Pedro de Martir complex (Gastil et al., 2014), eastern Peninsular Ranges batholith (EPRB) and Sierran suite complexes (e.g. Tuolumne complex; Memeti et al., 2010 and references therein; and Mt. Whitney complex; Hirt, 2007) of the Sierra Nevada batholith. With the exception of the non-cogenetic Border phase, the GCB consists mainly of granodioritic with less tonalitic and quartz dioritic compositions (Fig. 3), as does the EPRB and Sierran suite, although the Tuolumne complex does include a volumetrically insignificant mafic component.

(c) In addition to the Border phase, the GCB includes two temporally (2011 to 208 Ma), geochemically and petrogenetically distinct suites (Highland Valley and Bethleham). In this the GCB resembles the composite Tuolumne complex which includes at least three geochemically and isotopically distinct batches of magma (Kuna Crest, Half Dome and Cathedral Peak) emplaced over 10 My (95-85 Ma; Coleman et al., 2004).

(d) Partial melting modelling of GCB initial magmas indicated their derivation by high P-T partial melting of mafic protoliths with garnet stable and plagioclase unstable. This petrogenesis produces HREE-depleted and Sr-enriched magmas that exhibit the distinctive trace element signatures of SF plutonic suite, including elevated Sr/Y, La/Yb, Gd/Yb, and Gd/Yb. The viability of such a petrogenetic model has been substantiated by the Bissig et al. (2017) study of a restitic garnet-bearing granodiorite suite that generated Au-Cu porphyry mineralization. Almost all Highland Valley and Bethleham suite samples plot in the SF fields on discrimination diagrams developed by Hildebrand and Whalen (2014). However, most Border phase samples exhibit slightly lower La/Yb and Gd/Yb values than other GCB phases, possibly due to their containing cumulate amphibole, a HREE-enriched mineral that results in reduced La/Yb and Gd/Yb values. Alternatively, the 3 M.y. older Border phase may represent transitional arc to SF magmatism.

Some notable differences between the GCB and other Cordilleran slab failure plutonic suites are:

(a) The GCB's juvenile Sr and Nd isotopic signatures are in marked contrast to the evolved Sr and Nd isotopic signatures exhibited by other Cordilleran SF plutonic complexes (e.g., Eastern Peninsular

Ranges batholith; and Sierran Crest Tuolumne complex, Sierra Nevada batholith; Hildebrand and Whalen, 2014; 2017). However, the younger SF-related Coast Plutonic complex (CPC) of British Columbia exhibits similar juvenile isotopic characteristics to the GCB (Hildebrand and Whalen, 2017). In the case of the CPC, this has been attributed to a lack of old subcontinental lithospheric mantle beneath the juvenile arc Wrangellia terrane into which it was emplaced (op. cit.), an explanation which can also be applied to the Quenellia terrane that hosts the GCB. Other studied Cordilleran SF suites were products of collisions between arcs and pericratonic arcs or the NA continent that were underlain by Precambrian subcontinental lithospheric mantle from which their old, evolved isotopic signatures were derived (op. cit.).

(b) In contrast to other studied SF plutonic suites, almost all GCB samples plot in the arc field rather than the slab failure field on Sr/Y vs Nb/Y and Y vs Nb discrimination diagrams (Figs. 15a and 16). The exceptions are the Bethleham phase post-ore dyke and three out of four Gnawed Mountain subphase samples, the emplacement of which are most closely tied to the two main mineralizing events at 210.3 ± 0.8 Ma and between 209.1 and 208.6 Ma, respectively. This is interpreted as indicating stability during partial melting of a phase that retains Nb and Ta, likely titanite or rutile, that is generally unstable during petrogenesis of most other SF suites. In the context of identifying potentially fertile SF plutonic suites, it may be relevant that nearly half of Arizona Laramide porphyry Cu hosting intrusions exhibit similar low Nb/Y values, accompanied by variable Sr/Y and La/Yb signatures (Fig. 14)

Exposed lower crustal sections of arc crust, such as the Talkeetna arc in Alaska (de Bari and Coleman 1989), are characterized by complex mafic cumulate zones, often with significant amphibole accumulation (e.g., Greene et al., 2006). Talkeetna cumulate rocks are characterized by relatively high, but very variable, Sr/Y contents (77 ± 92) and LREE-depleted to flat REE patterns (La/Yb= 0.36 to 1.15; op. cit.; Fig. 12). Fractionation of these plagioclase-bearing cumulates would drive resulting liquids to lower Sr/Y, typical of arc fractionation trends, and not to high Sr/Y 'adakite' compositions (Davidson et al., 2007). However, remelting of previously accumulated mafic lower crustal cumulates and interstitial melts with these geochemical features could produce dacitic melt compositions with high Sr/Y, low to moderate La/Yb and low Y and HREE contents. Although such a petrogenesis need not involve elevated P-T garnet-stable conditions, as required for the partial melting models (Appendix 2), the involvement of deep crustal melting with residual garnet in porphyry deposit generation has been demonstrated elsewhere (cf., Kay and and Mpodozis, 2001; Bissig et al., 2017). Also, these mafic cumulates could have formed through assimilation-fractional crystallization (AFC) processes, during which they acquired upper plate isotopic signatures, either juvenile or old continental crustal, thus explaining the isotopic signatures of SF magmas. In this model, asthenospheric mantle-derived SF-related magmas would provide the major thermal flux required to drive partial melting of fertile mafic cumulate-rich lower crust. An alternative interpretation of the origin of the distinctive trace element and isotopic signatures of SF magmatism is that they are derived directly from, and acquired their signatures from, partial melting of subcontinental lithospheric mantle, again driven by thermal input from uprising asthenospheric mantle melts (Hildebrand and Whalen, 2017).

Although the above model can explain the timing and distinctive geochemical features of slab failure (SF) magmatism that host Cu porphyry mineralization, reasons why SF-related plutons are more likely to be fertile and earlier arc-related magmatism is typically barren of porphyry deposits (e.g. Kerman batholith of central Iran; Shafiei et al., 2009) requires some discussion. One possible reason is that water-rich lower crustal cumulate zones represent sources for both fluids and metals within an arc system (e.g., Davidson et al., 2007) and thus can contribute fertile hydrous, magmas. However, in the absence of the mantle-derived thermal pulse provided by SF, the normal heat flow within arcs is not sufficient to partially melt these fertile protoliths (Clemens and Vielzeuf, 1987). Also, as evidenced by microprobe major element analyses of mafic silicates from the various GCB plutonic phases and SHRIMP REE analyses of zircon (Davis, unpublished data), the fertile Bethleham suite is more oxidized and hydrous than the barren Highland Valley suite, features that facilitate metal separation, transport and deposition (Wang et al., 2014a, b; Bissig et al., 2017). Another reason could be that the major crustal uplift that follows slab detachment and SF magmatism changes a normally subaqueous low-standing arc magmatic setting (Hildebrand and Bowring, 1984) to a sub aerial high-standing post-collisional setting. It has long been recognized that some porphyry deposits form within high-standing continental margin or evolved (thick crustal) arc settings, such as the Andes, while others form within thinner crust oceanic arcs (e.g., Philippines and Papua New Guinea). In petrogenetic models for porphyry systems, it has even been proposed that they form within the magmatic roots of stratovolcanoes (Sillitoe, 1973). In contrast, VMS deposits are known to generally form in active subaqueous arc or back-arc settings, both of which represent quite thin crustal settings that are generally known to be poor targets for porphyry deposit exploration (see Whalen et al., 2016).

Development of GCB within Regional Framework

In southern Quesnel Terrane, the Guichon Creek Batholith (GCB) is associated with the Late Triassic to Early Jurassic, mainly volcanic, Nicola Group that developed from approximately ~220 Ma to 190 Ma. The group's magmatic record can be subdivided into three main phases of activity. The first phase is represented by subaqueous, low-K calc-alkaline volcanic rocks of the western Nicola Group (Mortimer, 1987). Regionally, these arc-type volcanic rocks are not well dated but are interpreted to be late Carnian (~217-224 Ma) to early to middle Norian (210-217 Ma), based on paleontological evidence (Monger, 1989; Beatty et al., 2006, Ray and Dawson, 2004). The ca 215.6 Ma GCB Border phase may represent the final stage of this arc magmatism. A magmatic gap between the time (216-208 Ma) of GCB plutonism and alkaline magmatism at 204 -200 Ma is suggested by the available geochronological data for the area (Breitsprecher et al., 2007). That period is marked by a widespread development of a loosely-dated, Norian (post 208 Ma)-Pleinsbachian regional unconformity between Upper Triassic strata (and unroofed GCB) and Lower Jurassic strata in Quesnel terrane (Beatty et al., 2006) and an analogous unconformity in Stikinia (Logan and Mihalynuk, 2014). Near the GCB, that event is manifest by batholithic fragments in Lower to Middle Jurassic Ashcroft Formation (Northcote, 1969; McMillan, 1976). Subsequent subaerial alkaline

magmatism lasted from 204 to ~198 Ma followed by a second apparent hiatus, or reduced magmatic flux, which was followed by a period of renewed calc-alkaline ± shoshonitic magmatism at 196-192 Ma, the Wildhorse magmatic suite of Breitsprecher et al. (2007). This includes the likely arc-related Rossland Group volcanic rocks and Thuya, Takomkane, Pennask, and Wildhorse batholiths. The latter represent areally extensive batholith complexes in Quesnel terrane and are less well-mineralized than the GCB. During that transition, the structural style varies from trans-tensional faulting (e.g., Lornex and Highland Valley faults) which localized mineralization at Valley (and so, active between 210-206 Ma) and Pleinsbachian contraction resulting in easterly-directed thrusting of Nicola Group over Ashcroft Formation, and of distal over proximal facies rocks of the Ashcroft Formation (Travers, 1982; Monger and McMillan, 1984).

Within the context of this evolutionary history, the GCB represents the youngest magmatic activity within the Late Triassic calc-alkaline phase of the Nicola arc. It developed synchronously with elements of trans-tensional faulting and immediately preceded the eastward shift to alkaline magmatism at ~204 Ma and slightly later eastward-directed thrusting within Quesnel terrane. The change in magma composition, apparent magmatic gap immediately following GCB plutonism, and eastward shift in intrusive centers, collectively support a temporal association of Highland Valley mineralization with a significant change in the dynamics of the subduction system. Parrish and Monger (1992) previously ascribed the change in the character and position of Nicola arc magmatism to flattening of an east dipping subduction zone that caused the arc to migrate eastward. As outlined and argued above, we interpret the GCB and its porphyry Cu deposits to reflect arc-arc collision followed by slab detachment and slab failure magmatism within a juvenile intraoceanic setting. The temporally linked eastward migration and alkaline character of the upper Nicola Group volcanic rocks and Copper Mountain plutonic suite likely reflects westward migration of the Rubia superterrane over the SF-derived linear plume of upwelling asthenospheric mantle during which low volume melting of subduction modified lithospheric mantle occurred. A post-collisional setting is also consistent with the Cu-Au mineralization associated with these plutonic centres (e.g., Richards, 2009). Our tectonic model resembles in many aspects that of Logan and Mihalynuk (2014) for these paired Early Mesozoic Cu-Mo and Cu-Au porphyry deposit belts. In this scenario, collisional events and slab breakoff initially caused melting of amphibole-bearing deep arc crust producing the high Sr/Y, La/Yb, Gd/Yb and Nb/Y in GCB magmas, followed by eastward stepping of the mantle heat source and generation of subduction-modified sub-arc lithosphere-derived alkaline magmas of the upper Nicola arc. The Norian-Pleinsbachian regional unconformity between the Upper Triassic and Lower Jurassic and unroofing and erosion of the late Triassic batholiths provide evidence for tectonic uplift, consistent with rebound following slab detachment. Reestablishment of westward directed subduction beneath a composite intra-oceanic arc occurred by 196 Ma, as evidenced by the Rossland volcanics and Wildhorse plutonic suite. Detailed testing of different tectonic scenarios requires an improved understanding of the stratigraphic, structural and geochemical evolution of the Late Triassic to Jurassic Nicola arc for which modern geochemical and geochronological data are lacking.

The timing of the GCB and associated mineralization at Highland Valley appear unique relative to other porphyry systems in the Late Triassic - Early Jurassic arcs within the Quesnel terrane. With the exception of Mount Lytton, located 40 km to the SE, there are no other reliably-dated plutons of comparable age to the GCB within Quesnel terrane (Breitsbrecher et al., 2007). Plutonic complexes with reported ages similar to that of the GCB include the 208 ± 6 Ma Heffley Creek pluton and the 209 ± 4.7 Ma age of the Tulameen ultramafic complex. The Heffley Creek age has recently been revised to 194 Ma (K. Breitbrecher 2010 pers. com.) making it considerably younger than the GCB, and similar to other large Early Jurassic plutons such as the Thuya, Takomkane, Pennask and Bromley plutons. Similarly, the published age of the Tulameen complex is imprecise and an alternative interpretation, based on the weighted mean of six overlapping $^{206}Pb/^{238}U$ ages at 204.2 ± 0.2 Ma, is permissive and consistent with the alkaline composition of the complex, placing it within the timeframe of other alkaline plutonic centres in Quesnel terrane.

Given the distribution of volcanic rocks correlative with the Nicola Group over 1000 km of strike length from California to BC (Mortimer, 1987), it would seem unlikely that the GCB is a solitary example of Late Triassic ca. 216-208 Ma plutonism in Quesnel. The absence of other contemporaneous plutonic centres along this segment of the arc could be due to burial beneath younger rocks, or uplift and erosion during later tectonic events associated with accretion to the west and/or Tertiary extension

Conclusions

New geochronology and geochemical data illuminate the characteristics of the Guichon Creek Batholith (GCB), a complex, composite intrusion within late Triassic volcanic and sedimentary rocks of the Nicola Group which hosts the most important porphyry Cu resource in the Canadian Cordillera. New geochronological data indicate intrusion of three geochemically distinct suites within the batholith over an 8 M.y. period (216-208 Ma). Mineralization within Highland Valley District developed over an approximately 4 M.y. period between 210 and 206 Ma represented by at least three distinct episodes of mineralization: (a) Bethlehem deposit formed over a less than 800 ka period at 210.3 Ma; (b) Highmont and Valley deposits generated within a 1.1 M.y. interval between 209.1 and 208.6 Ma and; (c) vein molybdenite mineralization in the Valley pit formed at 206 ± 1.2 Ma (Ash et al., 2007)

Our geochemical characterization of the Highland Valley and Bethlehem suites indicates that the three magmatic suites cannot simply be related to a common parental magma, but rather represent distinct magma batches derived from different source compositions with independent P-T conditions of melting. Mineralization at GCB coincides with a change in magma composition from the Highland Valley Suite to the Bethlehem suite. In general, the quantitative modelling shows the younger mineralization-related Bethlehem suite is more hydrous and more oxidized than the older barren Highland Valley suite, a relationship documented elsewhere (Wang et al., 2014 a, b). As discussed previously, geochemical changes within the GCB essentially replicate those documented on a regional scale within pre-, syn- to post-mineralization extrusive rocks of the central to southern Andean arc (Kay and Mpodozis, 2001; Hollings et

al., 2005). However, the models for tectonomagmatic changes in the Andean arcs being responsible for generating significant ('world class' or 'giant') Cu (±Au or Mo) porphyry deposits (Kay and Mpodozis, 2001; Kay et al., 1999; Hollings et al., 2005) are based on regional scale volcanic geochemical datasets, rather than on geochemical data from plutonic suites that actually host porphyry deposits. In contrast, the GCB represents a self-contained record of geochemical changes within temporally well-constrained plutonic phases cumulating in multiple mineralization events. Unlike these earlier Andes focused studies, we argue for a post-collisional slab-failure origin for porphyry deposit hosted by 'adakitic-like' plutonic suites of the GCB and consider it likely that this model is equally applicable to Andean porphyry districts.

Acknowledgements

This study was greatly assisted by access to the Highland Valley Mine site provided by TECK and to the help of the mine geologist, Dennis Merber. W.J. McMillan is thanked for sharing his time and expertise in guiding our field work and sample collection. Collaborative research by the senior author with Robert Hildebrand on Cordilleran slab failure processes helped improve this study. Linda Cataldo, Jule Peressini, Carole Lafontaine, Tom Pestaj and Nancy Joyce are thanked for their help carrying out the analytical work at the Geochronology lab, Geological Survey of Canada. Alex Zagorevski is thanked for a very helpful critical internal review. Kevin Byrne is thanked for some helpful critical input that significantly improved this manuscript. Funding for this work was provided by the Targeted Geoscience Intitiative 3 of the Geological Survey of Canada.

REFERENCES

Anderson, R.G., Plouffe, A., Ferbey, T., and Dunn, C.E., 2012, The search for surficial expressions of buried Cordilleran porphyry deposits; background and progress in a new Targeted Geoscience Initiative 4 activity in the southern Canadian Cordillera, Geological Survey of Canada, Current Research 2012-7, 15 p. doi:10.4095/290295

Ash, C. H., Reynolds, P. H. Creaser R. A., and Mihalynuk M. G., 2007, 40Ar/39Ar and Re-O Isotopic Ages for Hydrothermal Alteration and Related Mineralization at the Highland Valley Cu-Mo Deposit (NTS 092I), Southwestern British Columbia: Geological Fieldwork 2006, BC Ministry of Energy, Mines and Petroleum Resources. Report 2007-1: 19-24.

Baldwin, J. A., and Pearce J. A., 1982, Discrimination of productive and nonproductive porphyritic intrusions in the Chilean Andes: Economic Geology, v. 77, p. 664–674.

Beatty, T. W., Orchard M. J., and Mustard P. F., 2006, Geology and tectonic history of the Quesnel terrane in the area of Kamloops, British Columbia, *in* Colpron, M. and Nelson, J.L., eds. Paleozoic Evolution and Metallogeny of Pericratonic Terranes at the Ancient Pacific Margin of North America, Canadian and Alaskan Cordillera. Geological Association of Canada. Special Paper 45, p. 483-504.

Bissig, T., Leal-Mejia, H., Stevens, R.B., and Hart, C.J.R., 2017, High Sr/Y magma petrogenesis and the link to porphyry mineralization as revealed by garnet-bearing I-type granodiorite porphyries of the Middle Cauca Au-Cu Belt, Columbia: Economic Geology, v. 112, p. 551-568.

Black, L.P., Kamo, S.L., Allen, C.M., Davis, D.W., Aleinikoff, J.N., Valley, J.W., Mundilf, R., Campbell, I.H., Korsch, R.J., Williams, I.S., and Foudoulis, C., 2004, Improved 206Pb/238U microprobe geochronology by the monitoring of a trace element-related matrix effect: SHRIMP, ID-TIMS, ELA-ICP-MS and oxygen isotope documentation for a series of zircon standards: Chemical Geology, v. 205, p. 115–140.

Branchflower, J. D., 1971, Isotopic dating of copper mineralization at Alwin and Valley properties, Highland Valley, southcentral British Columbia. Unpublished BSc thesis, University of British Columbia, Vancouver, B.C, University of British Columbia: 83.

Breitsprecher, K., Scoates J.S., Anderson R.G., and Weis D., 2007, Geochemistry of Mesozoic intrusions, Quesnel and Stikine Terranes (NTS 082; 092; 093), south-central British Columbia: Preliminary characterization of sampled suites, *in* Geoscience BC Summary of Activities 2006, Geoscience BC, Report 2007-1, p. 247–258.

Byrne, K., Lesage, G, Gleeson, S.A., and Lee, R.G., 2017, Large-scale sodic-calcic alteration around porphyry copper systems: examples from the Highland Valley Copper district, Guichon batholith, south-central British Columbia, *in* Geoscience BC Summary of Activities 2016, Geoscience BC, Report 2017-1, p. 213–222.

Casselman, M. J., McMillan W. J., and Newman K. M., 1995. Highland Valley porphyry copper deposits near Kamloops, British Columbia. A review and update with emphasis on the Valley deposit. Porphyry Deposits of the Northwestern Cordillera of North America, *in* Schroeter, T. G., ed., Canadian Institute of Mining and Metallurgy. Special Volume 46, p. 161-191.

Cathles, L. M., and Shannon R., 2007, How potassium silicate alteration suggests the formation of porphyry ore deposits begins with the nearly explosive but barren expulsion of large volumes of magmatic water: Earth and Planetary Science Letters, v. 262, p. 92-108.

Clemens, J.D., and Vielzeuf, D., 1987, Constraints in melting and magma production in the crust: Earth and Planetary Science Letters, v. 86, p. 287–306.

Coleman, D.S., Gray, W., and Glazner, A.F., 2004, Rethinking the emplacement and evolution of zoned plutons: Geochronologic evidence for incremental assembly of the Tuolumne Intrusive Suite, California: Geology, v. 32, p. 433-436.

Colpron, M., Nelson J. A. L., and Murphy, D. C., 2007, Northern Cordilleran terranes and their interactions through time: GSA Today, v. 17, p. 4-10.

Cooke, D. R., Hollings P., and Walshe J. L., 2005, Giant porphyry deposits: Characteristics, distribution, and tectonic controls: Economic Geology, v. 100, p. 801-818.

D'Angelo, M., 2016, Geochemistry, petrography and mineral chemistry of the Guichon Creek and Nicola batholiths, southcentral British Columbia. unpublished M.Sc. thesis, Lakehead University, 421 p.

Davidson, J., Turner S., Handley H., Macpherson C., and Dosseto A., 2007, Amphibole "sponge" in arc crust?: Geology, v. 35, p. 787-790.

de Silva, S. L., and Gosnold, W. D., 2007, Episodic construction of batholiths: Insights from the spatiotemporal development of an ignimbrite flare-up: Journal of Volcanology and Geothermal Research, v. 167, p. 320-335.

Debari, S. M., and Coleman R. G., 1989, Examination of the deep levels of an island arc: evidence from the Tonsina ultramafic-mafic assemblage, Tonsina, Alaska: Journal of Geophysical Research, v. 94, p. 4373-4391.

Defant, M. J., and Drummond M. S., 1990, Derivation of some modern arc magmas by melting of young subducted lithosphere: Nature, v. 347, p. 662-665.

DePaolo, D. J., 1981, Neodymium isotopes in the Colorado Front Range and crust-mantle evolution in the Proterozoic: Nature, v. 291, p. 193-196.

Diakow, L., 2010, The Spences Bridge Project: Mesozoic geology and mineralization in the Merritt region, southern B.C., Association for Mineral Exploration B.C. Roundup 2010, Volume 2010 Abstract: Vancouver, B.C., p. 33.

Gastil, R.G., Kimbrough, D.L., Kimbrough, J.M., Grove, M., and Shimizu, M., 2014, The Sierra San Pedro Mártir zoned pluton, Baja California, Mexico, *in* Morton, D.M., and Miller, F.K., eds., Peninsular Ranges Batholith, Baja California and Southern California: Geological Society of America Memoir, 211, p. 739–758.

Greene, A.R., DeBari, S.M., Kelemen, P.B., Blusztajn, J., and Clift, P.D., 2006, A detailed geochemical study of island arc crust; the Talkeetna Arc section, South-Central Alaska: Journal of Petrology, v. 47, p. 1051-1093.

Frost, B.R., Barnes, C.G., Collins, W.J., Arculus, R.J., Ellis, D.J., and Frost, C.D., 2001, A geochemical classification for granitic rocks: Journal of Petrology, v. 42, p. 2033-2048.

Frost, B.R., and Frost, C.D., 2008, A geochemical classification for feldspathic igneous rocks: Journal of Petrology, v. 4**9**, p. 1955-1969.

Hildebrand, R.S., 2010, Did Westward Subduction Cause Cretaceous-Tertiary Orogeny in the North America Cordillera?: Geological Society of America Special Paper 457, 71p.
Hildebrand, R.S., 2013, Mesozoic Assembly of the North American Cordillera: Geological Society of America Special Paper 495, 169p.
Hildebrand, R. S., and Bowring, S. A., 1984, A non-extensional model for the origin of continental intra-arc depressions, with a Proterozoic example from Wopmay orogen, Northwest Territories, Canada: Geology, v. 12, p. 73-77.
Hildebrand, R.S., and Whalen, J.B., 2014, Arc and slab-failure magmatism in Cordilleran batholiths II – The Cretaceous Peninsular Ranges batholith of Southern and Baja California: Paul Hoffman Volume, Geoscience Canada, v. 41, p. 399-458.
Hildebrand, R.S., and Whalen, J.B., 2017, The Tectonic Setting and Origin of Cretaceous Batholiths within the North American Cordillera: The Case for Slab Failure Magmatism and Its Significance for Crustal Growth: Geological Society of America Special Paper 532, p. 1–113
Hildreth, W., and Moorbath, S., 1988, Crustal contributions to arc magmatism in the Andes of Central Chile: Contributions to Mineralogy and Petrology, v. 98, p. 455-489.
Hirt, W.H., 2007, Petrology of the Mount Whitney Intrusive Suite, eastern Sierra Nevada, California: Implications for the emplacement and differentiation of composite felsic intrusions: Geological Society of America Bulletin, v. 119, p. 1185–1200, http://dx.doi.org/10.1130/B26054.1.
Hollister, V.F. Allen, J.M. Anzalone, S.A., and Seraphim, R.H., 1975, Structural evolution of porphyry mineralization at Highland Valley, British Columbia: Canadian Journal of Earth Sciences, v. 12, p. 807-820.
Hollings, P., Cooke, D., and Clark, A., 2005, Regional geochemistry of Tertiary igneous rocks in central Chile: Implications for the geodynamic environment of giant porphyry copper and epithermal gold mineralization: Economic Geology, v. 100, p. 887-904.
Johnston, S.T., 2008, The Cordilleran ribbon continent of North America: Annual Review of Earth and Planetary Sciences, v.36, p. 495-530.
Jones, M.B., Schmuck, R.A., and Field, C.W., 1973, K-Ar dates from the Valley copper and Lornex deposits, Guichon Creek Batholith, Highland Valley district, British Columbia: Isochron West, v. 7, p. 17-20.
Jourdan, F., and Renne, P.R., 2007, Age calibration of the Fish Canyon sanidine 40Ar/39Ar dating standard using primary K-Ar standards: Geochimica et Cosmochimica Acta, v. 71, p.387-402.
Kay, S.M., Godoy, E., and Kurtz, A., 2005, Episodic arc migration, crustal thickening, subduction erosion, and magmatism in the south-central Andes: Bulletin of the Geological Society of America, v. 117, p. 67-88.
Kay, S.M., and Mpodozis, C., 2001, Central Andean Ore deposits linked to evolving shallow subduction systems and thickening crust: GSA Today, v. 11, p. 4-9.
Kay, S.M., Mpodozis, C., and Coira, B., 1999, Eogene magmatism, tectonism and mineral deposits of the central Andes, *in* Skinnner, B., ed., Geology and Ore Deposits of the Central Andes. Society of Economic Geology Special Publication, v. 7, p. 27-59.
Krogh, T.E., 1982. Improved accuracy of U-Pb zircon ages by the creation of more concordant systems using an air abrasion technique: Geochimica et Cosmochimica Acta, v. 46, p. 637-649.
Lang, J.R., Lueck, B., Mortensen, J.K., Russell, J.K., Stanley, C.R., and Thompson, J.F.H., (1995, Triassic-Jurassic silica-undersaturated and silica-saturated alkalic intrusions in the cordillera of British Columbia: implications for arc magmatism: Geology, v. 23, p. 451-454.
Lang, J.R., and Titley, S.R., 1998, Isotopic and geochemical characteristics of Laramide magmatic systems in Arizona and implications for the genesis of porphyry copper deposits: Economic Geology, v. 93, p. 138-170.
Lee, R.G., Dilles, J.H., Tosdal, R.M., Wooden, J.L., and Mazdab, F.K., 2017, Magmatic evolution of granodiorite intrusions at the El Salvador porphyry copper deposit, Chile, based on trace element composition and U-Pb age of zircons: Economic Geology, v. 112, p. 245-273.
Lipman, P.W.A., 2007, Incremental assembly and prolonged consolidation of Cordilleran magma chambers; evidence from the Southern Rocky Mountain volcanic field: Geosphere, v. 3, p. 42-70.
Logan, J.M., Mihalynuk, M.G., Ullrich, T., and Friedman, R.M., 2007, U-Pb ages of intrusive rocks and $^{40}Ar/^{39}Ar$ plateau ages of copper-gold-silver mineralization associated with alkaline intrusive centres at Mount Polley and the Iron Mask batholth, southern and central British Columbia:

Geological Fieldwork 2006, BC Ministry of Energy, Mines and Petroleum Resources Report 2007-1, p. 93-116.
Logan, J.M., and Mihalynuk, M.G., 2014, Tectonic controls on Early Mesozoic paired alkaline porphyry deposit belts (Cu-Au ± Ag-Pt-Pd-Mo) within the Canadian Cordillera: Economic Geology, v. 109, p. 827-858.
Macpherson, C.G., Dreher, S.T., and Thirlwall, M.F., 2006, Adakites without slab melting: High pressure differentiation of island arc magma, Mindanao, the Philippines: Earth and Planetary Science Letters, v. 243, p. 581-593.
Martin, H., Smithies, R.H., Rapp, R., Moyen, J.-F., and Champion, D., 2005, An overview of adakite, tonalite-trondhjemite-granodiorite (TTG), and sanukitoid: Relationships and some implications for crustal evolution: Lithos, v. 79, p. 1-24.
Mattinson, J.M., 2005, Zircon U–Pb chemical abrasion ("CA-TIMS Q") method: Combined annealing and multi-step partial dissolution analysis for improved precision and accuracy of zircon ages; Chemical Geology, v. 220, p.47–66.
McMillan, W.J., 1976, Geology and genesis of the Highland Valley ore deposits and the Guichon Creek Batholith, Canada, *in* Sutherland Brown, A., ed., Porphyry deposits of the Canadian Cordillera. Canadian Institute of Mining and Metallurgy. Special Volume 15, p.85-104.
McMillan, W.J., 1985, Geology and ore deposits of the Highland Valley Camp: Geological Association of Canada, Mineral Deposits Division, Field Guide and Reference Manual Series. Number 1, 121 p.
McMillan, W.J., and Johan, Z., 1981, Geochemistry of the Guichon Creek Batholith, British Columbia, Canada, *in* Silberman, M., Field, C., and Berry, A., eds., Proceeding of the symposium on mineral deposits of the Pacific Northwest, 1980. Reston, VA, United States Geological Survey, Open File Report 81-355, p. 84-105.
McMillan, W.J., Anderson, R.G., Chen, R., and Chen, W., 2009, Geology and mineral occurrences (MINFILE), the Guichon Creek Batholith and Highland Valley porphyry copper district, British Columbia: Geological Survey of Canada, Open File 6079.
McMillan, W.J., Thompson, J.F.H., Hart, C.J.R., and Johnston, S.T., 1996, Porphyry deposits of the Canadian Cordillera: Geoscience Canada, v. 23, p. 125-134.
Memeti, V., Paterson, S., Matzel, J., Mundil, R., and Okaya, D., 2010, Magmatic lobes as "snap- shots" of magma chamber growth and evolution in large, composite batholiths: An example from the Tuolumne intrusion, Sierra Nevada, California: Geological Society of America Bulletin, v. 122, p. 1912–1931, doi:10.1130/B30004.1.
Monger, J.W.H., 1989b. Geology, Ashcroft, British Columbia. Geological Survey of Canada, Map 7 42-1989, Scale 1:250,000.
Monger, J.W.H., and McMillan, W.J., 1984, Bedrock geology of Ashcroft (92 I, map. Geological Survey of Canada, Open File Report 980; map, charts and notes.
Monger, J., and Price, R., 2002, The Canadian Cordillera: Geology and Tectonic Evolution: Canadian Society of Geophysicists Recorder, v. 27, p. 17-36.
Monger, J.W.H., Price, R.A., and Tempelman-Kluit, D.J., 1982, Tectonic accretion and the origin of the two major metamorphic and plutonic welts in the Canadian Cordillera: Geology, v. 10, p. 70-75.
Mortimer, N., 1986, Late Triassic, arc-related, potassic igneous rocks in the North American Cordillera: Geology, v. 14, p. 1035-1038.
Mortimer, N., 1987, The Nicola Group: Late Triassic and Early Jurassic subduction-related volcanism: Canadian Journal of Earth Sciences, v. 24, p. 2521–2536.
Mortimer, N., van der Heyden, P., Armstrong, R.L., and Harakal, J., 1990, U-Pb and K-Ar dates related to the timing of magmatism and deformation in the Cache Creek Terrane and Quesnellia, southern British Columbia: Canadian Journal of Earth Sciences, v. 27, p. 117-123.
Moyen, J.-F., 2009, High Sr/Y and La/Yb ratios: The meaning of the "adakitic signature": Lithos, v. 112, p. 556-574.
Moyen, J.-F., and Stevens, G., 2006, Experimental constraints on TTG petrogenesis: Implications for Archean geodynamics: American Geophysical Union Geophysical Monograph, v. 164, p. 149-175.
Northcote, K.E., 1969, Geology and geochronology of the Guichon Creek Batholith: British Columbia Ministry of Energy Mines and Petroleum Resources Bulletin 56, 73p.
Parrish, R. R., and Monger, J. W. H., 1992, New U-Pb dates from southwestern British Columbia: Geological Survey of Canada, Paper 91-2, p. 87–108

Parrish, R.R., Roddick, J.C., Loveridge, W.D., and Sullivan, R.W., 1987, Uranium - lead analytical techniques at the Geochronology Laboratory: Geological Survey of Canada Paper, v. 87-02, p. 3-7.

Pearce, J.A., Harris, N.B.W., and Tindle, A.G., 1984, Trace element discrimination diagrams for the tectonic interpretation of granitic rocks: Journal of Petrology, v. 25, p. 956–983.

Preto, V. A., Osatenkom, O.M., McMillan, W.J., and Armstrong, R.L., 1979, Isotopic dates and strontium isotopic ratios for plutonic and volcanic rocks in the Quesnel Trough and Nicola Belt, South-central British Columbia, Canada: Canadian Journal of Earth Sciences, v. 16, p. 1658 - 1672.

Preto, V. A., 1977, The Nicola Group; Mesozoic volcanism related to rifting in southern British Columbia, *in* Baragar, W.R.A., Coleman, L.C., and Hall, J.M., eds., Volcanic regimes in Canada. *Edited by* Geological Association of Canada, Special Paper *16*, pp. *39-57.*

Ray, G.E., and Dawson G, L., 1994, The geology and mineral deposits of the Hedley gold skarn district, southern British Columbia: British Columbia Ministry of Energy Mines and Petroleum Resources Bulletin 87, 156p

Ray, G.E., Dawson, G.L., and Webster, I.C.L., 1996, The stratigraphy of the Nicola Group in the Hedley district, British Columbia, and the chemistry of its intrusions and Au skarns: Canadian Journal of Earth Sciences, v. 33, p. 1105-1126.

Renne P. R., Deino A. L.,Walter, R.C., Turrin, B.D., Swisher C. C., Becker, T. A., Curtis, G. H., Sharp, W. D., and Jaouni, A-R.,1994, Intercalibration of astronomical and radioisotopic time: Geology v. 22, p. 783-786.

Richards, J.P., 2009, Post subduction porphyry Cu-Au and epithermal Au deposits: Products of remelting of subduction-modified lithosphere: Geology, v. 37, p. 247-250.

Richards, J.P., and Kerrich, R., 2007, Adakite-like rocks: Their diverse origins and questionable role in metallogenesis: Economic Geology, v. 102, p. 537-576.

Ricketts, B.D., Evenchick, C.A., Anderson, R.G., and Murphy, D.C., 1992, Bowser basin, northern British Columbia: Constraints on the timing of initial subsidence and Stikinia-North America terrane interactions: Geology, v.20, p. 1119-1122.

Roddick, J.C., 1987, Generalized numerical error analysis with applications to geochronology and thermodynamics: Geochimica et Cosmochimica Acta, v. 51, p. 2129-2135.

Roddick, J.C., 1988, The assessment of errors in $^{40}Ar/^{39}Ar$ dating. In: Radiogenic Age and Isotopic Studies, Report 2. Geological Survey of Canada, Paper 88-2, p. 7–16.

Roddick, J.C., Cliff, R.A., and Rex, D.C., 1980, The evolution of excess argon in alpine biotites — a $^{40}Ar/^{39}Ar$ analysis: Earth and Planetary Science Letters, v. 48, p. 185–208.

Roy, B., and Clowes, R.M., 2000, Seismic and potential-field imaging of the Guichon Creek batholith, British Columbia, Canada, to delineate structures hosting porphyry copper deposits: Geophysics, v. 65, p. 1418-1434.

Sajona, F.G., Maury, R.C., Prouteau, G., Cotten, J., Schiano, P., Bellon, H., and Fontaine, L., 2000, Slab melt as metasomatic agent in island arc magma mantle sources, Negros and Batan (Phillipines): Island Arc, v. 9, p. 472-486.

Scaillet, S., 2000, Numerical error analysis in $^{40}Ar/^{39}Ar$ dating: Chemical Geology, v.162, p. 269–298.

Schau, M.P., 1970, Stratigraphy and structure of the type area of the Upper Triassic Nicola Group in south-central British Columbia, *in* Wheeler, J.O., ed., Structure of the Southern Canadian Cordillera, Special Paper 6, Geological Association of Canada, p. 123–135.

Shafiei, B., Haschke, M., and Shahabpour, J., 2009, Recycling of orogenic arc crust triggers porphyry Cu mineralization in Kerman Cenozoic arc rocks, southeastern Iran: Mineralium Deposita, v. 44, p. 265-283.

Sillitoe, R.H., 1973, The tops and bottoms of porphyry Cu deposits: Economic Geology, v. 68, p. 799-815.

Smith, A.D., Brandon, A.D., and Lambert, R.S., 1995, Nd-Sr isotope systematics of Nicola Group volcanic rocks, Quesnel terrane: Canadian Journal of Earth Sciences, v. 32, p. 437-446.

Stern, R.A., 1997, The GSC Sensitive High Resolution Ion Microprobe (SHRIMP): analytical techniques of zircon U-Th-Pb age determinations and performance evaluation: *in* Radiogenic Age and Isotopic Studies: Report 10, Geological Survey of Canada Current Research 97-F, p. 1-31.

Stern, R.A., and Amelin, Y., 2003, Assessment of errors in SIMS zircon U-Pb geochronology using a natural zircon standard and NIST SRM 610 glass: Chemical Geology, v. 197, p. 111-142.

Streckeisen, A.L., and LeMaitre, R.W., 1979, Chemical approximation to modal QAPF classification of the igneous rocks: Neus Jahrbuch fur Mineralogie, v. 136, p. 169-206.

Stormer, J.C., and Nicolls, J., 1978, XLFRAC: a program for the interactive testing of magmatic differentiation models: Computers and Geoscience, v. 4, p. 143-159.
Struik, L.C., Schiarizza, P., Orchard, M.J., Cordey, F., Sano, H., MacIntyre, D.G., Lapierre, H., and Tardy, M., 2001, Imbricate architecture of the upper Paleozoic to Jurassic oceanic Cache Creek Terrane, central British Columbia: Canadian Journal of Earth Sciences, v. 38, p. 495-514.
Sun, S.-S., and McDonough, W.F., 1989, Chemical and isotopic systematics of oceanic basalts: implications for mantle composition and processes, *in* Saunders, A.D., and Norry, M.J., eds., Magmatism in the Ocean Basins. Geological Society Special Publication, Blackwell Scientific, p. 313-345.
Travers, W, 1978, Overturned Nicola and Ashcroft strata and their relation to the Cache Creek Group, southwestern Intermontane Belt, British Columbia: Canadian Journal of Earth Science, v. 15, p. 99-116.
Travers, W., 1982, Possible large scale thrusting near Ashcroft, British Columbia: Implications for petroleum prospecting: Bulletin of Canadian Petroleum Geology, v. 30, p. 1-8.
Villeneuve, M.E., and MacIntyre, D.G, 1997, Laser $^{40}Ar/^{39}Ar$ ages of the Babine porphyries and Newman Volcanics, Fulton Lake map area, west-central British Columbia: in *Radiogenic Age and Isotopic Studies, Report 10*. Geological Survey of Canada, Current Research 1997-F: p. 131–139.
Villeneuve, M.E., Sandeman, H.A., and Davis, W.J., 2000, A method for the intercalibration of U-Th-Pb and $^{40}Ar/^{39}Ar$ ages in the Phanerozoic.: Geochimica et Cosmochimica Acta, v. 664, p. 4017-4030.
Wang, R., Richards, J.P., Hou, Z., Yang, Z., and DuFrane, S.A., 2014a, Increased magmatic water content - The key to Oligo-Miocene porphyry Cu-Mo±Au formation in the eastern Gangdese Belt, Tibet: Economic Geology, v. 109, p. 1315-1339.
Wang, R., Richards, J.P., Hou, Z., Yang, Z., Guo, Z. and DuFrane, S.A., 2014b, Increasing magmatic oxidation state from Paleocene to Miocene in the eastern Gangdese Belt, Tibet: Implications for collision-related porphyry Cu-Mo±Au mineralization: Economic Geology, v. 109, p. 1943-1965.
Wanless, R.K., 1973, Age determinations and geological studies, K-Ar Isotopic Ages, Report 11: Geological Survey of Canada Paper 73-2, p. 8-114.
Wanless, R.K., Stevens, R.D., Lachance, G.R., and Rimsaite, J.Y.H., 1965, Age determinations and geological studies; Part 1-Isotopic ages, Report 5: Geological Survey of Canada, Paper 64-17, p.11-126.
Wanless, R.K., Stevens, R.D., Lachance, G.R., and Rimsaite, J.Y.H., 1968, Age determinations and geological studies: Geological Survey of Canada Paper 67-2A, p.11-141.
Whalen, J.B., Anderson, R.G., Struik, L.C., and Villeneuve, M.E., 2001, Geochemistry and Nd isotopes of the Francois Lake plutonic suite, Endako batholith: Host and progenitor to the Endako molybdenum camp, central British Columbia: Canadian Journal of Earth Sciences, v. 38, p. 603-618.
Whalen, J.B., and Frost, C.D., 2013, The Q-ANOR diagram: A tool for the petrogenetic and tectonomagmatic characterization of granitic suites: Geological Society of America, *Abstracts with Programs*, v. 45, no. 3, p. 24.
Whalen, J.B., Pehrsson, S.J., and Rayner, N.M., 2016, Significance of pre-1860 Ma granitoid magmatism for crustal evolution and exploration targeting in the Flin Flon assemblage, Trans-Hudson orogen, Canada: Economic Geology, v. 111, p. 1021-1039.
White,W.H., Ericksong, P., Northcotek, E., Dirom, G.E., and Harakalj, E., 1967. Isotopic dating of the Guichon batholith, British Columbia: Canadian Journal of Earth Sciences, v. 4, p. 677-690.
Woodsworth, G.A., Anderson, R.G., and Armstrong, R.L., 1992, Plutonic regimes, *in* Gabrielse, H., and Yorath, C.J., eds., Geology of the Cordilleran orogen in Canada, Volume G-2: Boulder, CO, Geological Society of America, p. 491-531.